ACS OMEGA

Open Access

http://pubs.acs.org/journal/acsodf

Article

Nanocellulose-Based Ecofriendly Nanocomposite for Effective Wastewater Remediation: A Study on Its Process Optimization, Improved Swelling, Adsorption, and Thermal and Mechanical Behavior

Harshdeep Rana, Anamika, Dipti Sareen,* and Saswata Goswami*

Cite This: *ACS Omega* 2024, 9, 8904−8922

Read Online

ACCESS | Metrics & More | Article Recommendations | Supporting Information

ABSTRACT: A nanocellulose (NC)-based cross-linked adsorbent has been employed herein for the removal of dye pollutants (e.g., methylene blue) from the textile industry. The synthesized hydrogel was optimized to achieve the best concentrations of the adsorbent constituents, i.e., 1.55% guar gum, 1.46% NC, and 0.84% borax for achieving the maximum swelling index (SI, 3741.42%) and higher adsorption capacity (q_e, 24.05 mg g^{-1}). 98.8% of dye q_e was achieved at optimal conditions of pH 8 within 30 min at 30 °C. Adsorption isotherms and kinetics investigations showed good correlation with the Freundlich adsorption isotherm model (R^2 > 0.9889; $\Delta G^\circ = -4.71$; $\Delta H^\circ = -12.30$; $\Delta S^\circ = -0.025$) as well as the pseudo-second-order kinetics model, indicating multilayered and intricate adsorption mechanisms for dye removal. The study of thermodynamic parameters confirmed the exothermic nature of the adsorption process. The adsorption−desorption study of the resulting hydrogel exhibited 64.58% dye removal efficiency even after 4 consecutive cycles of reuse. Further, scanning electron microscopy, Fourier transform infrared spectroscopy, thermogravimetric analysis, and X-ray diffraction analysis revealed the surface morphology, functional moieties, thermal behavior, and crystallinity pattern of the hydrogel. Rheological analysis demonstrated pseudoplastic flow and improved mechanical behavior for the hydrogel. The current study found that the synthesized adsorbent with a higher SI and q_e has a noticeable potential for the removal of dye pollutants from wastewater.

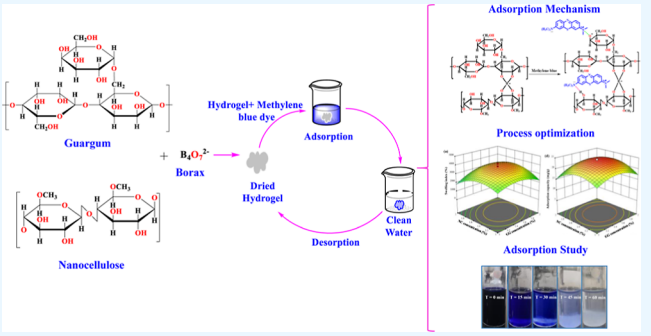

1. INTRODUCTION

Industrial and domestic wastewater is the major source of water pollution and has emerged as one of the most significant environmental issues. According to World Bank reports, approximately 17−20% of industrial wastewater is generated by the textile industry. In India, due to the high global demand for polyester and cotton, the textile industry consumes approximately 80% of total production (approximately 1,30,000 tons) of dye stuff.[1] Like various dyes, methylene blue (MB) is one of the main hazardous wastes released from the textile industry that can seriously pollute water bodies, posing threat to aquatic and human life. Therefore, it is crucial to discover an efficient and sustainable method to reduce the potential hazards imposed by these textile dyes.

The adsorption method is one of the most effective approaches due to its low cost, high efficiency, ease of design, superior stability, and flexibility.[2] Various metal oxide-, carbon-, polymer-, and biopolymer-based adsorbents are already in use for the removal of dye contaminants from wastewater.[3,4] Currently, biopolymer-based formulations have become an effective and innovative approach because of their strong biocompatibility, biodegradability, renewability, water retention capacity, and affordability.[5]

Hydrogels are 3D cross-linked polymeric structures that can absorb significant amount of water without getting dissolved. Hydrogels are currently used specifically to remove dye pollutants via adsorption mechanisms through various interactions such as electrostatic attraction, ion exchange, hydrogen bonding, etc.[6] Various synthetic materials used in the formulation of hydrogels encompass poly(vinyl alcohol) (PVA), polylactic acid (PLA), polycaprolactone (PCL), polyethylene glycol (PEG), etc. Despite their potential utility, use of these materials has been constrained due to concerns related to their biodegradability and potential toxicity, emphasizing sustainability and safety.[7,8] Therefore, natural

Received: September 11, 2023
Revised: December 29, 2023
Accepted: January 5, 2024
Published: February 13, 2024

https://doi.org/10.1021/acsomega.3c06924
ACS Omega 2024, 9, 8904−8922

biopolymers, such as cellulose, chitosan, guar gum (GG), starch, pectin, and alginate, and their derivatives are currently being explored for dye adsorption applications because of their relative abundance and characteristics like surface area, pore size, and pore volume. Biopolymers with modified surfaces exhibit improved chemical and thermal stability, stiffness, flexibility, and quick responsiveness.[5]

Among these, GG and its cross-linked derivatives have shown great potential as flocculating agents, making them excellent candidates for hydrogel formation for wastewater treatment, drug delivery, and biosensor applications. GG offers several advantages over other polysaccharides for hydrogel formation, such as self-assembling properties, biocompatibility, low cost, pH sensitivity, hydrophilicity, nontoxicity, etc.[6,9] Despite these, GG still has some limitations for their scope of applications, such as weak structural integrity, mechanical properties, and restricted durability, that can be addressed by incorporating various reinforcing materials or nanoparticles, such as carbon nanotubes, clay, metal-based nanoparticles like ferritin, etc.[10] Among several reinforcements, nanocellulose (NC) stands out as the most promising and eco-friendly solution to mitigate the limitations of GG. In the current study, indigenous surface-modified NC (industrial apple pomace-derived) was used as the nanofiller. NC enables better interaction with the matrix because of its larger specific surface area, low density, high crystallinity, and high strength-to-weight ratio.[11] Previously, intense efforts have been made to improve the durability, reliability, and mechanical properties of hydrogels with the incorporation of NC.[4,11−14] All of these approaches have demonstrated significant improvement in mechanical properties at low filler loadings. The current study exclusively relies on biodegradable natural resources for the selection of hydrogel components. The superior gelling property of GG and the enhanced mechanical properties of surface-modified NC render this biodegradable self-reinforced nanocomposite highly suitable for wastewater remediation. Moreover, NC used in this study is itself derived from industrial fruit waste, making this innovative approach more sustainable, promoting the idea of waste recyclability for wastewater remediation.

Several GG-based hydrogels have been reported for the removal of dye pollutants from wastewater, such as aniline dye,[15] Congo red dye,[16] Acid Red 8 (AR8) dye,[17] crystal violet, azure B dye,[18] etc. The efficient adsorption of MB dye has also been explored through GG-based hydrogels, such as the TiO_2-embedded GG hydrogel (R % = 96%),[19] PANI-incorporated GG-acrylic acid (SI = 1376%; R = 88%)-based cross-linked hydrogel,[20] galactomannan acrylamide-octadecyl methacrylate hydrogel (SI = 2340%; q_e = 19.3 mg g^{-1}),[21] and GG-poly(acrylic acid−aniline)-based interpenetrating hydrogel network (SI = 2345.06%; R % = 93.87%)[22] but with limited swelling and adsorption or dye removal capabilities. NC-based hydrogels for the removal of MB dye include tannin-immobilized cellulose (TC) hydrogels (R % = 80%; q_e = 0.40 mg g^{-1})[23] and cross-linked poly(2-methacryloyloxyethyl phosphorylcholine) (PMPC)/bacterial nanocellulose (BNC) composite (SI = 912%; q_e = 4.5 mg g^{-1}).[24] Despite the fact that GG- and NC-based hydrogels have individually been widely explored, the NC-incorporated GG-based self-reinforced hydrogels have rarely been studied for the removal of dye contaminants.

The widely used cross-linkers to produce hydrogels, which include glutaraldehyde, epichlorohydrin, glyoxal, and formaldehyde, often face difficulties with high toxicity, poor biodegradability, biocompatibility, and solubility.[25] However, the rare exception to all these limitations is the use of borax (BX) as an eco-friendly cross-linking agent. Previously, BX has already been effectively used to produce cross-linking in a variety of hydrogels, including cellulose-,[26] starch-,[27] PVA,[11] and GG-based hydrogels,[15] but rare combinations of BX have been found in GG/NC-based hydrogels.

From the scientific literature review, it was clear that the ability of hydrogel composites to absorb is not enough without modifications, like the addition of a suitable cross-linker. This is because there are too many H-bonds between the hydroxyl groups of polymers. This will consequently hinder its ability to adsorb and ion exchangeability in the dye solution. To overcome such limitations, many efforts have been made to develop efficient adsorbents, but very few studies are available on NC-incorporated cross-linked hydrogels for effective dye removal applications. Here, we have tried to develop a novel eco-friendly GG-based hydrogel nanocomposite, incorporated with apple pomace-derived surface-modified cellulose nanoparticles as a filler (NC) and a biodegradable, nontoxic cross-linker (BX) to maximize its swelling index (SI) and dye adsorption capacity (q_e).

The aim of this research work is to fabricate a GG/NC-based cross-linked hydrogel via a simple dissolution method and optimize the process conditions (i.e., GG, NC, and BX concentration) to enhance its swelling and q_e. Physicochemical properties, such as the SI, biodegradability, reusability study, q_e (at different initial dye concentrations, pHs, temperatures, and times), morphological analysis, crystallinity, thermal stability, and rheological properties were investigated. To figure out how the cross-linked hydrogel adsorbed, we also looked at its adsorption kinetics, adsorption isotherm, and thermodynamic behavior.

The use of waste-derived modified NC as a filler and BX as a cross-linking agent to produce an adsorbent with high SI and adsorption capacity would be a sustainable and innovative approach for water remediation. In the current study, we tried to emphasize the challenges faced by GG- and NC-based individual hydrogels. The current research work revealed higher physiochemical, thermal, and mechanical properties as compared to the previously reported hydrogels.

2. MATERIALS AND METHODS

2.1. Materials. GG and BX were purchased from Loba Chemie Ltd., India. The surface-modified crystalline NC was prepared in our lab. BX, acetone, and ethanol were purchased from Central Drug House Pvt. Ltd. (New Delhi, India). Hydrochloric acid, sodium hydroxide, sulfuric acid, urea, dipotassium hydrogen phosphate, and MB were purchased from Merck Life Science Pvt. Ltd. (Mumbai, India). All the reactions were carried out in distilled water.

2.2. Experimental Section. *2.2.1. Process Optimization of the Cross-Linked Hydrogel.* The cross-linked hydrogel was prepared through simple dissolution and polymerization methods. Response surface methodology (RSM)-based central composite design (CCD) was applied to study the effect of different concentrations of independent factors such as GG (X_1), NC (X_2), and BX (X_3) on the responses. The responses, i.e., the SI (%) and q_e (mg g^{-1}) of the hydrogel were denoted "Y_1"and "Y_2", respectively. The three independent factors, i.e., GG (0.5−2.5%, w/v), NC (0.5−2.5%, w/v), and BX (0.25−1.25%, w/v) were varied at 5 levels (−2, −1, 0, +1, +2)

https://doi.org/10.1021/acsomega.3c06924
ACS Omega 2024, 9, 8904−8922

consisting of 20 experimental runs (Table 1). Design-Expert software, version 13.0.5.0 (Stat-Ease Inc., Minneapolis, USA)

Table 1. Coded Levels for the Independent Factors of the Hydrogel Composite

			levels				
factor	code	unit	−2	−1	0	1	2
GG concentration	X_1	%	0.5	1.0	1.5	2.0	2.5
NC concentration	X_2	%	0.5	1.0	1.5	2.0	2.5
BX concentration	X_3	%	0.25	0.5	0.75	1.0	1.25

was employed for the design of experiments and statistical data analysis. Analysis of variance (ANOVA) was used to study the significance and adequacy of the regression model.

GG was physically copolymerized with NC and BX to form a uniform hydrogel solution. A homogeneous solution of 0.310 g of GG was prepared in 20 mL distilled water under stirring for 2 h at room temperature so that GG solution can completely hydrate and attain maximum viscosity. Similarly, 0.292 g of NC was dispersed and 0.168 g of BX was dissolved separately in 20 mL of distilled water and stirred for 30 min at room temperature. BX solution and NC dispersion were added one by one to GG solution with continuous stirring for 30 min at 50 °C. After mixing, the synthesized hydrogel was kept aside for another 4 h and then rinsed with distilled water to eliminate unreacted BX. For dehydration, the hydrogel was soaked in acetone for 16 h and then oven-dried at 45 °C (Figure S1).

2.2.2. Determination of Unreacted BX. To estimate the concentration of unreacted BX in the hydrogel sample, the back-titration method was used with some modifications following previous literature.[15,28] For that, 0.2 g of hydrogel was dissolved in distilled water (100 mL). After that, 2 to 3 drops of methyl red indicator were added to the above dispersion and titrated against 0.01 M HCl solution. The change in dispersion color from yellow to pink was considered as an end point. The end point reading observed for GG solution was recorded as blank, and the value was subtracted from the value recorded for the hydrogel. To estimate the cross-linked BX, the above cross-linked hydrogel dispersion was preheated at 70 °C to break the cross-linked bonds between them, followed by similar titration. The amount of unreacted and cross-linked BX was estimated from the volume of HCl solution used by considering 1 mol of BX equivalent to 2 mol of HCl.

2.3. Physiochemical Properties. *2.3.1. Water Content, Swelling Index, and Gel Fraction.* The cross-linked hydrogel was initially weighed (w_i) and then incubated in distilled water until a constant weight was achieved (for equilibrium SI). After removing unrestrained surface water, the swollen hydrogel was weighed (w_s).[15,26] Finally, the swollen hydrogel was dried and weighed (w_d). The water content (WC), swelling index (SI), and gel fraction (GF) of hydrogel were determined using eqs 1−3, respectively

$$\mathrm{WC} = \frac{w_s - w_i}{w_s} \times 100\% \quad (1)$$

$$\mathrm{SI} = \frac{w_s - w_i}{w_i} \times 100\% \quad (2)$$

$$\mathrm{GF} = \frac{w_d}{w_i} \times 100\% \quad (3)$$

2.3.2. Surface Area Analysis. The adsorption process is significantly influenced by the surface chemistry of the adsorbent. The specific surface area, average pore diameter, and pore volume of the hydrogel were determined following a previously described method.[29] The analysis was performed by the Brunauer−Emmett−Teller (BET) method with the Quantachrome Instruments Autosorb iQ station 1, version 5.21 using the gas (N_2) adsorption isotherm relative pressure (p/p_0) of 0.01 to 0.99. The hydrogel sample (40 mg) was degassed in vacuum at 100 °C for 5 h before carrying out the analysis. The bath temperature of 77.35 °C was provided for 2−3 h for the sample analysis.

2.3.3. Biodegradability. To check the biodegradability of hydrogel, 0.25 g (w_o) of hydrogel sample was incubated in a soil extract solution (100 mL) for 10 days. The soil extract solution was obtained as described in previous literature.[4] After 10 days, the residual filtrate of hydrogel was collected, oven-dried at 60 °C for 4 h, and weighed (w_f). The weight loss of the hydrogel sample was determined using eq 4

$$\text{weight loss} = \frac{w_o - w_f}{w_o} \times 100\% \quad (4)$$

2.3.4. Recyclability. The recyclability study of hydrogel was performed by immersing 0.02 g of dry hydrogel in MB dye solution (30 mg L^{-1}) for saturated adsorption at pH 7 at room temperature. After that, the hydrogel (dye loaded) was immersed in 0.1 M HCl for 4 h and rinsed with ethanol and distilled water, respectively. This used hydrogel was reused for the next dye adsorption cycle per above-described procedure until it completely degraded.[19]

2.4. Adsorption Study of MB Dye on Hydrogel. The degree of dye adsorption was determined by immerging 0.02 g of hydrogel sample in 10 mL of aqueous solution of MB dye (30 mg L^{-1}) for 60 min. The effects of initial dye concentration, pH, temperature, and contact time on dye removal percentage (R %) were investigated in this study. A Cytation 5 Cell Imaging Multimode Reader (Agilent BioTek) was used to measure the before and after adsorption concentrations of MB dye in solution within the wavelength range of 400−800 nm. The adsorption value of MB dye was changed to the concentration by a linear regression equation generated through the calibration curve over different concentrations. The MB removal percentage (R) was estimated from eq 5

$$R = \frac{C_0 - C_t}{C_0} \times 100\% \quad (5)$$

While q_t and q_e (mg g^{-1}), the adsorption capacities of the MB dye at a particular time and at equilibrium, respectively, were calculated using eqs 6 and 7, respectively

$$q_t = \frac{(C_0 - C_t) \times V}{m} \quad (6)$$

$$q_e = \frac{(C_0 - C_e) \times V}{m} \quad (7)$$

where C_0 is the dye concentration (mg L^{-1}) at initial time and C_t (mg L^{-1}) is the dye concentration (mg L^{-1}) at time t; V is the volume (L) of the dye solution used; m is the dried weight (g) of the cross-linked hydrogel.

https://doi.org/10.1021/acsomega.3c06924
ACS Omega 2024, 9, 8904−8922

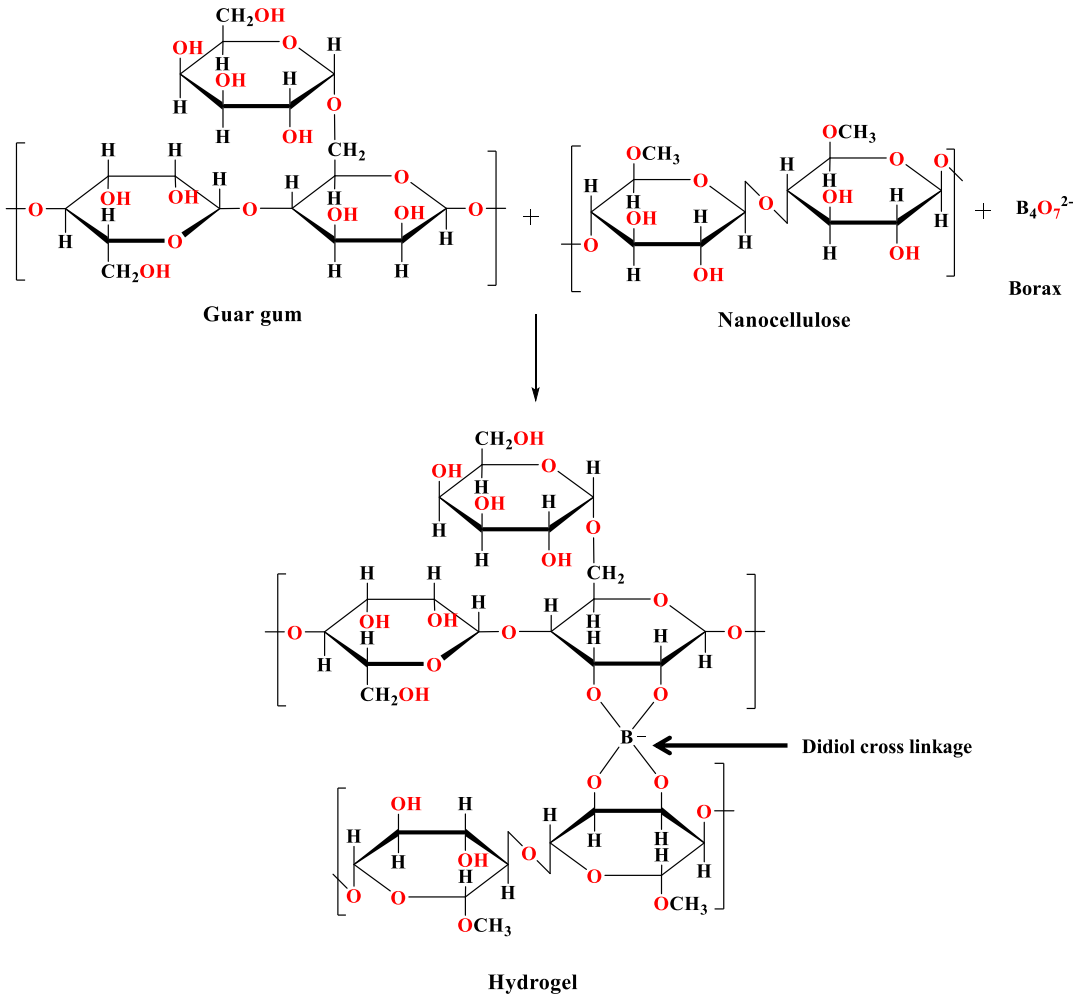

Figure 1. Cross-linking mechanism of the BX-cross-linked GG/NC-based hydrogel forming a didiol complex.

The study of adsorption kinetics was conducted at different concentrations (30−50 mg L^{-1}) of dye on its removal percentage. In an effort to investigate the impact of initial dye concentration, 0.02 g of dry hydrogel was soaked in 10 mL of dye solution with a pH of 7.0 for a contact time of 60 min at room temperature. Similarly, the impact of various contact times (15−60 min) was examined by introducing 0.02 g of dry hydrogel into 10 mL of MB dye solution (30 mg L^{-1}) at pH 7.0 and room temperature. To check the impact of solution pH (4−9) on *R* %, 0.02 g of dry hydrogel was added into 10 mL of MB solution (30 mg L^{-1}) for 60 min at room temperature.

The adsorption isotherm and thermodynamic analyses were carried out at different temperatures (30−50 °C) by adding 0.02 g of hydrogel into 10 mL of MB solution (30 mg L^{-1}) at pH 7.0. After a contact time of 60 min, the final concentration of MB dye solution was analyzed.[13,22]

2.5. Characterization. The structure and surface morphology of the hydrogel were investigated using scanning electron microscopy (SEM; JEOL JCM 6000 Nikon Corporation) at an accelerated voltage of 10 kV. To identify functional groups of the hydrogel composite, Fourier transform infrared spectroscopy with attenuated total reflection (FTIR-ATR) analysis was performed using an Agilent Technologies Cary 600 instrument with a resolution of 4 cm^{-1} in the range of 400−4000 cm^{-1}. Thermogravimetric analysis (TGA; simultaneous thermal analyzer (STA) 8000) at a temperature interval of 30−800 °C with the uniform heating rate of 10 °C/min under the nitrogen atmosphere was employed to examine the thermal stability of the hydrogel. X-ray diffraction (XRD) analysis was performed to find the phase composition (crystallinity or amorphous) and thereby the chemical composition of the cross-linked hydrogel. The samples were analyzed with the high-speed position sensitive detector system in a Cu X-ray tube device with a Ni filter and scanned over a range of 2θ values of 5−60° at 5 °C/min rate. The degree of crystallinity (CI) was determined by eq 8

$$\mathrm{CI} = \frac{I_{\mathrm{Crystalline}} - I_{\mathrm{Amorphous}}}{I_{\mathrm{Crystalline}}} \times 100\% \quad (8)$$

where $I_{\mathrm{Crystalline}}$ represents the area of crystalline regions and $I_{\mathrm{Amorphous}}$ the amorphous regions.

2.6. Rheological Studies. Rheological analysis of the hydrogel was performed using a dynamic mechanical analyzer (MCR 702) fitted with a parallel-plate geometry (d = 50 mm and 1.0 mm gap size) at room temperature. In oscillatory analysis, the amplitude or strain sweep test was analyzed at a fixed frequency of 1 Hz to determine the linear elastic region to define the rheological stability within the strain range of 0.01−1000%. The storage modulus (G', Pa) and loss modulus (G'', Pa) were also examined to better understand the viscous/elastic properties of the hydrogel using frequency sweep tests (0.01−1000 rad s^{-1}) at a fixed shear strain of 1%.

https://doi.org/10.1021/acsomega.3c06924
ACS Omega 2024, 9, 8904−8922

Table 2. CCD Model for the SI and Dye q_e of the NC-Based Hydrogel with Experimental and Predicted Values

				SI (%) Y_1		q_e (mg g^{-1}) Y_2	
run no.	GG conc. (%) X_1	NC conc. (%) X_2	BX conc. (%) X_3	experimental value	predicted value	experimental value	predicted value
1	2	2	1	2409.9	2199.02	17.22	16.3098
2	1.5	1.5	0.75	3797.5	3799.96	24.2	24.1097
3	1.5	1.5	1.17045	2671.2	2843.5	19.13	19.8374
4	1.5	2.3409	0.75	1242.1	1519.2	12.75	13.0254
5	2	1	1	2399.5	2285.35	17.47	17.5676
6	1.5	1.5	0.329552	1508.6	1447.8	13.02	12.3216
7	1	2	1	1617	1496.9	13.59	13.675
8	2	1	0.5	1047.2	1120.46	11.42	11.3287
9	2	2	0.5	2699.5	2497.23	15.25	15.7109
10	1.5	1.5	0.75	4174.2	3799.96	24.5	24.1097
11	1.5	0.659104	0.75	1775	1609.4	14.23	13.758
12	0.659104	1.5	0.75	1817.7	1697.23	14.36	14.1086
13	1	2	0.5	934.7	970.01	11.08	11.9752
14	2.3409	1.5	0.75	2191.5	2423.47	16.48	16.7403
15	1.5	1.5	0.75	3591.2	3799.96	23.71	24.1097
16	1	1	0.5	858.9	990.94	9.93	10.8339
17	1.5	1.5	0.75	3724	3799.96	24.3	24.1097
18	1.5	1.5	0.75	3672	3799.96	23.58	24.1097
19	1.5	1.5	0.75	3860	3799.96	24.37	24.1097
20	1	1	1	2825.5	2948.93	19.64	19.1728

2.7. Statistical Analysis. All the experiments were conducted in triplicate, and results are presented as a mean value, as well as bar graphs were shown with the error bar. Design-Expert software, version 13.0.5.0 (Stat-Ease Inc., Minneapolis, USA) was used for ANOVA analysis with significant statistical difference of up to $p < 0.05$.

3. RESULTS AND DISCUSSION

3.1. Cross-Linking Mechanism and Process Optimization for Hydrogel Synthesis. BX is a dynamic cross-linking agent that dissociates into trigonal boric acid ($B(OH)_3$) and a tetrahydroxy borate ion $[B(OH)_4]^-$ in aqueous solution. These ions react with functional groups such as −OH groups of polymers to form didiol cross-links (boron ester bonds) that enhances the thermal and mechanical properties of hydrogels.[27] The high pH range of the solution facilitates higher $[B(OH)_4]^-$ ion formation, which also leads to a stronger cross-linking reaction and ultimately higher mechanical properties of the composite. In the present study, $[B(OH)_4]^-$ of BX was physically cross-linked with −OH groups of GG and NC, forming the didiol cross-links (Figure 1).

Optimization of process parameters for hydrogel synthesis through CCD of RSM was carried out as summarized in Table 2. The best 20 experimental conditions comprise three factors; therefore, three levels central composite response surface designs were selected. The empirical relationship was assessed between the independent factors and the effect of their interactions on responses, i.e., SI (%, Y_1) and q_e (mg g^{-1}; Y_2). The three independent factors for hydrogel fabrication were decided with a fixed solid−liquid ratio (SLR) (1:20) level. Table S2 represents the lowest and the highest SI (Y_1) as well as q_e (Y_2) under various experimental conditions. The mathematical model equations for SI and q_e were obtained using the CCD model given by eqs 9 and 10, respectively

$$\mathrm{SI} = +3799.96 + 215.91X_1 - 26.82X_2 + 414.95X_3 + 349.43X_1X_2 - 198.28X_1X_3 - 365.77X_2X_3 - 615.05X_1^2 - 790.43X_2^2 - 584.89X_3^2 \quad (9)$$

$$q_e = +24.11 + 0.7824X_1 - 0.2789X_2 + 2.23X_3 + 1.06X_1X_2 - 0.5250X_1X_3 - 1.41X_2X_3 - 3.07X_1^2 - 3.75X_2^2 - 2.84X_3^2 \quad (10)$$

ANOVA was used to check the significance level and accuracy of the fitted model for hydrogel preparation, and the results are given in Table S1. The determination coefficient (R^2) for SI (i.e., 0.9741) and q_e (i.e., 0.9917) of the cross-linked hydrogel (Table S1) were found much higher and exhibited a high degree of relationship between the experimental and predicted values. The adequate precision value of 16.6737 (SI) and 29.3831 (q_e) along with coefficient of variation (CV %) of 9.83% (SI) and 3.65% (q_e) were also found significant. In the present study, the higher F-values of 41.72 and 67.24 (SI and q_e, respectively) as well as low P-values of <0.0001 specified that the predicted quadratic models were significant ($P < 0.05$). Furthermore, nonsignificant lack of fit also validated the predicted quadratic models for the current study. 3D response surface plots (Figure 2) have been used as the function of GG (X_1), NC (X_2), and BX (X_3) concentrations to explain the interactions and relationships between these independent factors and dependent factors.

3.1.1. Effect of Independent Parameters on the SI of Hydrogel. The SI between 858.9% and 4174.2% (Table 2) of the hydrogel composite with varying concentrations of process parameters were found in accordance with previous NC- and GG-based hydrogel studies.[4,15,17] Figure 1a−c explains the effect of parameters on SI, where the incorporation of GG (0.5−1.55% w/v), NC (0.5−1.47% w/v), and BX (0.25−0.83% w/v) in terms of their interaction demonstrated remarkable improvement in SI. However, on increasing or

https://doi.org/10.1021/acsomega.3c06924
ACS Omega 2024, 9, 8904−8922

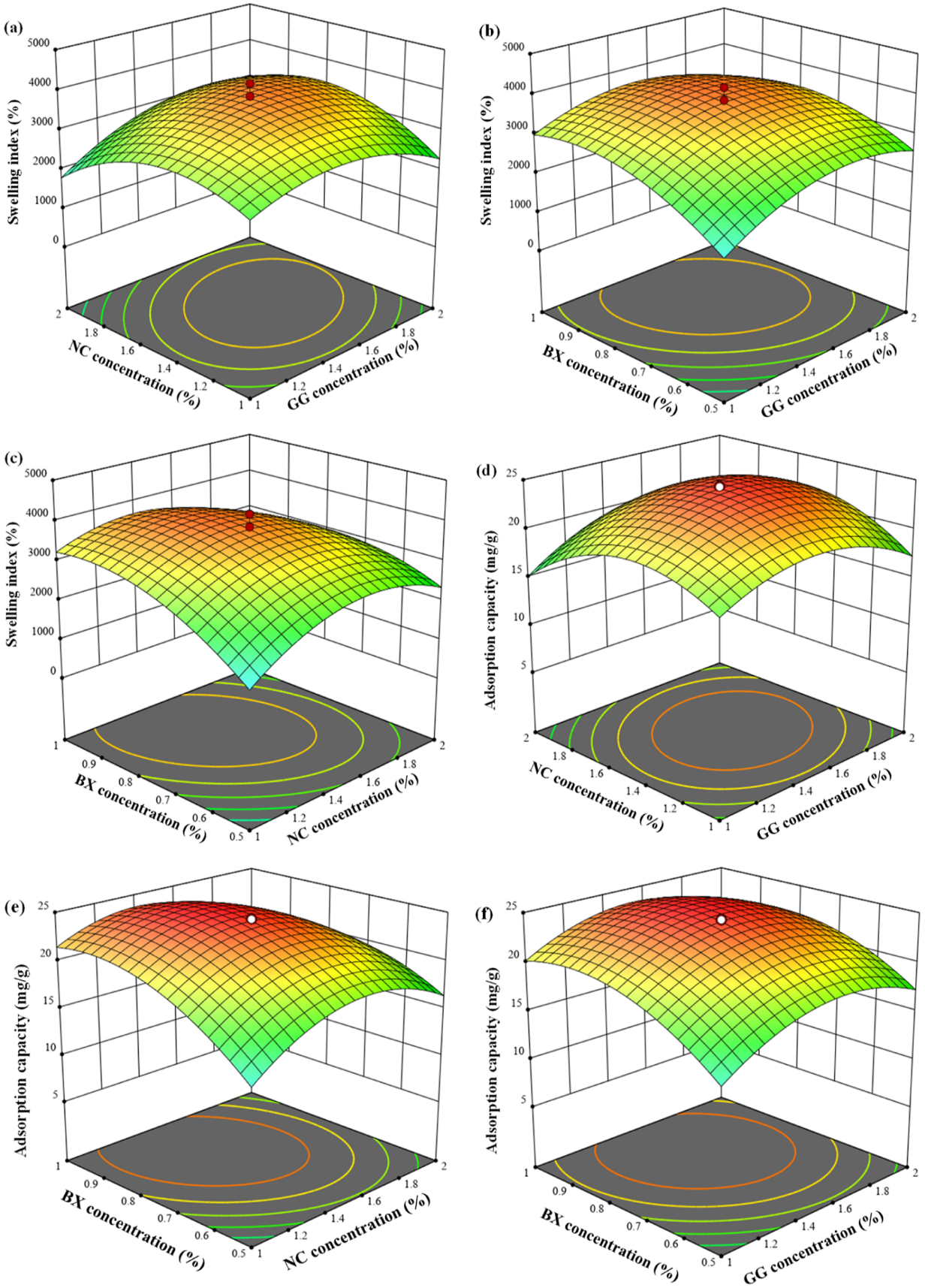

Figure 2. 3D contour graphs of the (a−c) effect of individual parameter on the SI and (d−f) effect of individual parameter on the q_e of the fabricated GG/NC-based hydrogel.

https://doi.org/10.1021/acsomega.3c06924
ACS Omega 2024, 9, 8904−8922

Table 3. Validation of the CCD Model for Cross-Linked Hydrogel Preparation

process parameters			SI (%)		q_e (mg g^{-1})	
GG conc. (%)	NC conc. (%)	BX conc. (%)	experimental values	predicted values	experimental values	predicted values
1.55	1.46	0.84	3741.42	3886.7	24.05	24.61

Table 4. Back-Titration Calculation of Unreacted and Cross-Linked BX in Hydrogel Samples

sample code	volume of hydrochloric acid (mL) required at room temperature (a)	$b = a -$ blank	concentration of unreacted BX (mg/200 mg)	volume of hydrochloric acid (mL) required after heating (c)	$d = c -$ blank	concentration of cross-linked BX calculated from "d" (mg/200 mg)
$GG_{1.55}$	1.0 (blank)					
$GG_{1.55}/NC_{1.46}$	1.0 (blank)					
$GG_{1.55}/BX_{0.84}$	1.4	0.3	11.5	4.5	3.5	13.7
$GG_{1.55}/NC_{1.46}/BX_{0.84}$	1.3	0.2	0.766	4.8	3.8	16.2

decreasing the concentrations of constituents, a reduction in SI was observed. The excellent hydrophilicity of the hydrogel constituents, i.e., GG and NC has been demonstrated by the cross-linked networks and the presence of rich hydrophilic groups.[6] GG has robust interactions with cellulose derivatives and water molecules that impart viscosity and thickening to the solution.[30] Besides this, the incorporation of BX has also resulted in a substantial increase in SI. This momentous improvement in SI is attributed to the generation of $B(OH)^{4-}$ that reacts with the −OH groups of biopolymers to form didiol cross-links through hydrogen bonding which is associated with the polymer bridging as well as the porous structure of hydrogel. Thus, an improvement has been noticed for the cross-linked network of hydrogel upon addition of BX (0.25−0.83% w/v). However, the cross-linking effect of BX decreased with a further increase in the BX concentration, which indicates the generation of stronger electrostatic repulsion in the hydrogel as more sites of GG and NC hydroxyl groups were occupied by $B(OH)^{4-}$.[31]

According to Table S1, the regression coefficients for linear GG (X_1), BX (X_3), quadratic (X_1^2, X_2^2, X_3^2), as well as interactive terms (X_1X_2, X_1X_3, X_2X_3) have shown a noteworthy effect ($p < 0.05$) on the SI value, whereas the linear term regression coefficient for NC (X_2), did not show an important effect on SI ($p > 0.05$). The model has generated eq 9 to predict SI using specified ranges of independent factors, where positive values of the regression coefficient exhibited positive effects and negative values indicated negative effects on the SI response. Ideal concentrations were observed for cross-linked hydrogel components, i.e., 1.55% GG, 1.46% NC, and 0.84% BX, to achieve the maximum SI. Recently, a NC-based hydrogel has reported an SI of 2770% (within 4−5% NC concentration) and hypothesized that smaller hydrogel pores induced by increased NC concentrations may have contributed to the reduction in SI, which clearly limits the entry of extra water molecules into the hydrogel network.[4]

3.1.2. Effect of Independent Parameters on the q_e of Hydrogel. The q_e of hydrogel composites were scrutinized to investigate the maximum R % value under varying concentrations of process parameters. The q_e of cross-linked hydrogels were found to be between 9.93 and 24.5 mg g^{-1} (Table 2) with a R % of 39.72−98% at a dosage of 0.05 mg/10 mL aqueous medium at an initial concentration. These outcomes of the present investigation were found in accordance with the previous results of GG- and NC-based hydrogels.[4,17] Figure 1d−f explains the effect of addition of parameters, i.e., GG (1.55% w/v), NC (1.46% w/v), and BX (0.84% w/v) on q_e in terms of their interactions, indicating the outstanding improvement in q_e as well as R %. However, q_e and R % values decreased upon lowering or exceeding specific concentrations of independent parameters. The initial increase in R % is attributable to the availability of active −OH sites on the hydrogel for ionic interaction with the MB dye. The availability of adsorption sites decreased upon increase of the contact time of the adsorbent and dye which might have occurred because of the saturation of the active adsorption sites. Similarly, on increasing the BX concentration (up to 0.84%), more borate ions got generated and eventually contributed to the charge neutralization of deprotonated dye molecules. Similar outcomes were reported in a previous article, where R % of aniline blue dye got saturated above 15% of BX concentration in the case of cross-linked GG BX hydrogel.[15]

The regression coefficients for linear, quadratic, as well as interacting factors have demonstrated a notable effect (p 0.05) on the q_e value (Table S1); however, the NC (X_2), linear term regression coefficient did not reveal that much influence on q_e ($p > 0.05$). The suggested model has produced eq 10 to predict q_e using selected ranges of parameters that indicated positive or negative effects on q_e response per their sign (+ or −). It can be concluded that q_e were also substantially affected by the independent parameters of the hydrogel. The ideal parameter concentrations to achieve the maximum q_e were 1.55% w/v GG, 1.46% w/v NC, and 0.84% w/v BX. In a recent study, a NC-based hydrogel was reported with a q_e of 17.72 mg g^{-1} using 4−5% NC concentration,[4] which is less than the present study.

3.1.3. Model Validation. The accuracy of the predicted model for response was ensured by the results obtained under optimal conditions, as given in Table 3. Under optimum conditions (trial no. 1), i.e., 1.55% of GG concentration, 1.46% of NC concentration, and 0.84% of BX concentration, 3741.42% of SI and 24.05 mg g^{-1} of q_e were obtained, which was very close to the predicted value (96.28% for SI and 97.72% for q_e). Therefore, the given method for the hydrogel preparation with a higher SI with enhanced q_e showed utmost efficiency. It is noteworthy that the hydrogel with a higher SI was achieved along with enhanced q_e in comparison to the earlier reported results.[4,17]

3.2. Unreacted BX Estimation. The amount of unreacted BX in hydrogel samples was estimated by the back-titration method, as shown in Table 4. In contrast to $GG_{1.55}/BX_{0.84}$, the unreacted BX concentration in the NC-incorporated hydrogel ($GG_{1.55}/NC_{1.46}/BX_{0.84}$) was considerably reduced by 93.34%. Additionally, the cross-linked BX concentrations for $GG_{1.55}/BX_{0.84}$ and $GG_{1.55}/NC_{1.46}/BX_{0.84}$ were estimated to be 13.7 and 16.2 mg, respectively. The higher concentration of cross-linked

https://doi.org/10.1021/acsomega.3c06924
ACS Omega 2024, 9, 8904−8922

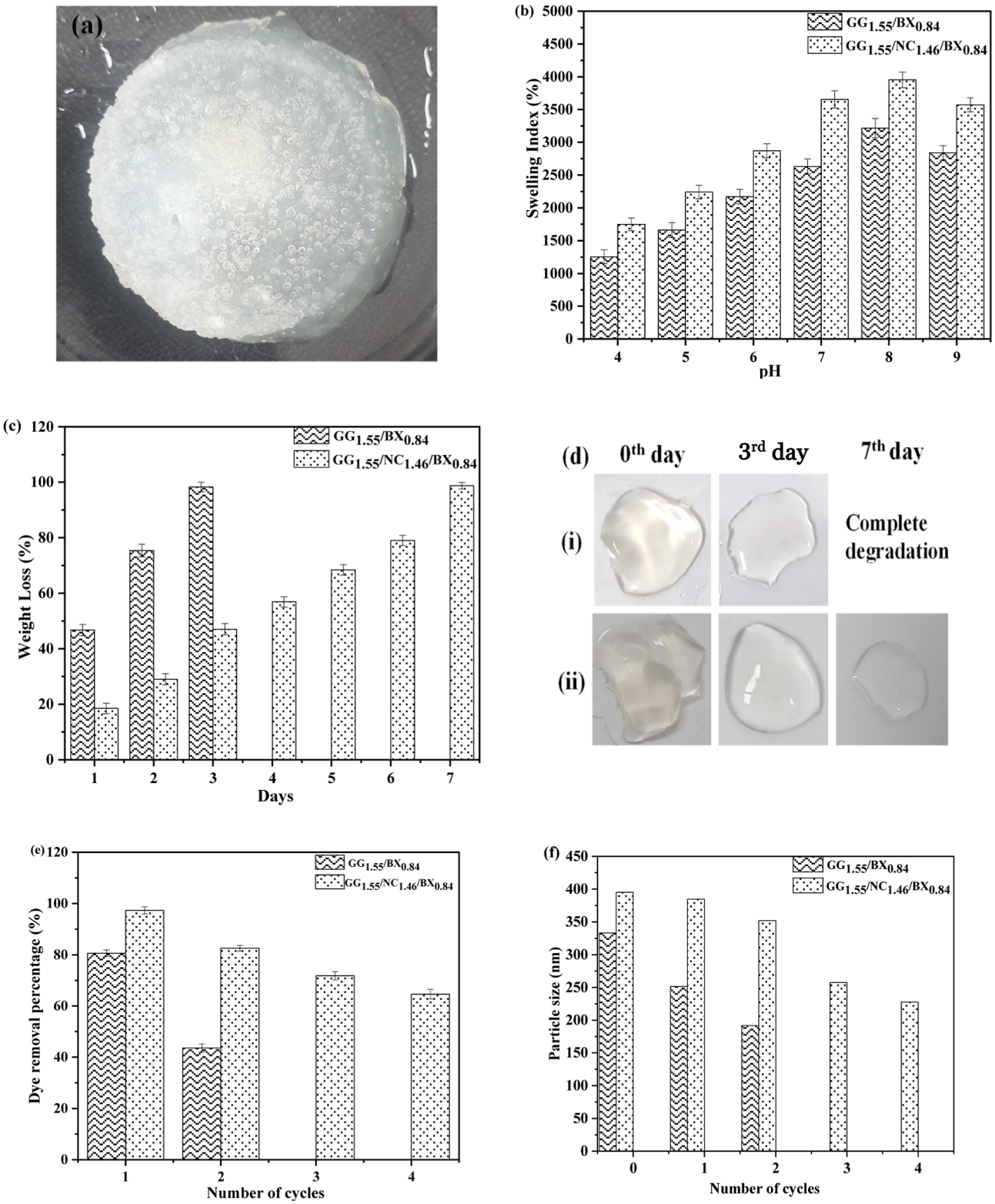

Figure 3. (a) Gel appearance, (b) SI (%), (c) biodegradability (weight loss %), (d) digital images of (i) $GG_{1.55}/BX_{0.84}$ and (ii) $GG_{1.55}/NC_{1.46}/BX_{0.84}$ biodegradable hydrogels, and (e) recyclability analysis.

BX in $GG_{1.55}/NC_{1.46}/BX_{0.84}$ may have been caused by the abundant reactive −OH groups and high surface area of the hydrogel induced by cellulose nanoparticles. More active sites will allow more BX to get cross-linked, which could result in lesser amounts of unreacted BX. Per prior investigation of GG BX-based hydrogel, the concentration of unreacted and cross-linked BX was found to increase with the increased concentration of BX up to 20%.[15]

3.3. Physiochemical Properties. *3.3.1. Water Content, Swelling Index, and Gel Fraction.* The $GG_{1.55}/BX_{0.84}$ hydrogel was able to retain water up to 88.2%, while the incorporation of filler (NC) into the hydrogel ($GG_{1.55}/NC_{1.46}/BX_{0.84}$)

https://doi.org/10.1021/acsomega.3c06924
ACS Omega 2024, 9, 8904−8922

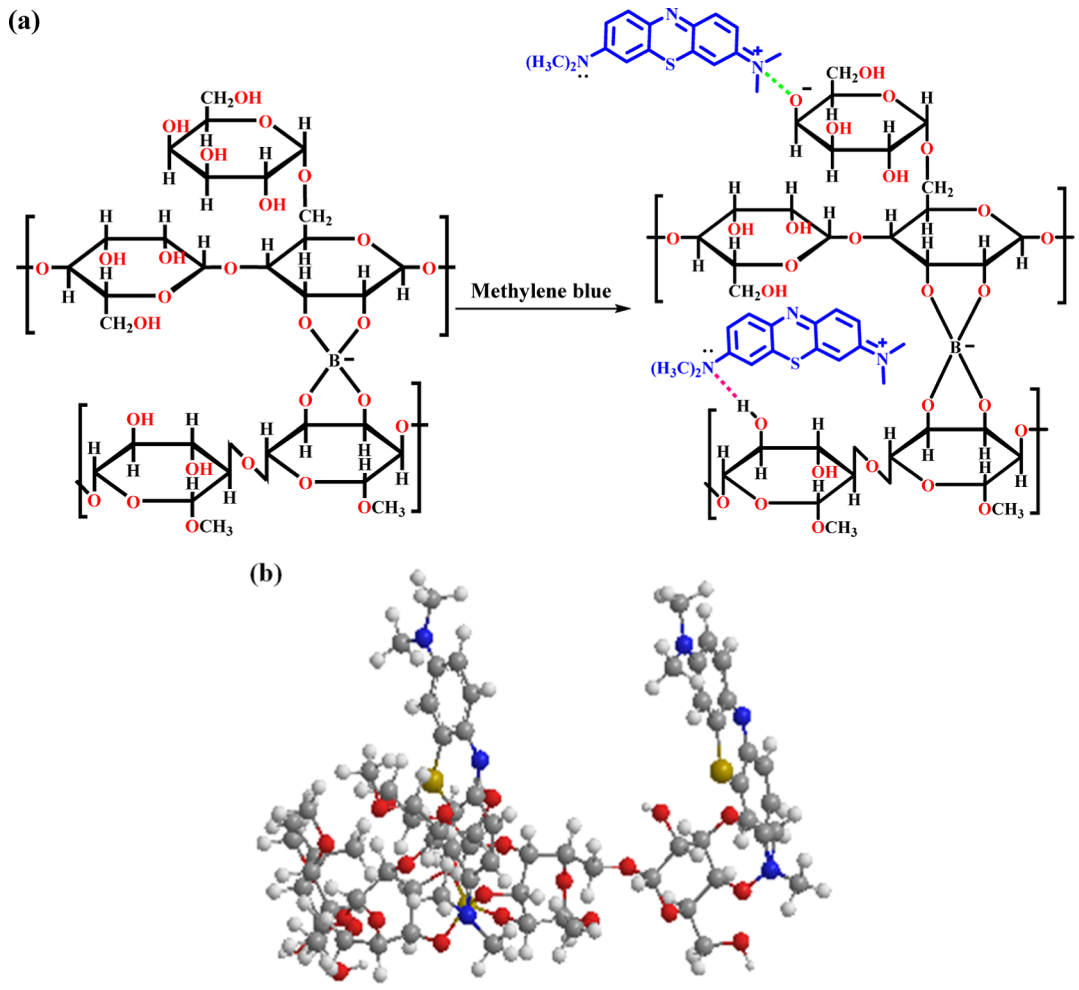

Figure 4. (a) Proposed mechanism of MB dye adsorption via electrostatic interaction (green hyphen) and H-bonding (red hyphen) on the $GG_{1.55}$/$NC_{1.46}$/$BX_{0.84}$ hydrogel surface and (b) 3D structure of the MB-adsorbed hydrogel composite.

increased the WC % value up to 95.4% under neutral pH. This could be described by the presence of additional hydroxyl groups of NC and the development of a cross-linked didiol complex that interacts with water molecules. A recent study showed that integration of BX into a cellulose-based hydrogel increased the WC % of hydrogel from 90.8 to 93.0%.[26] At higher BX loadings, higher amount of water could be obtained in the hydrogel composites. Besides that, the higher amount of solid content in the hydrogel can also lead to a lower WC in contrast to the hydrogel with a lower solid content.[32]

The swelling ability of hydrogel generally depends on factors, including the immersion time, polymer constituents, solvent, specific surface area, amount of cross-linker, pore size, and hydrophilic groups present in hydrogels.[17] In this study, SI for hydrogels ($GG_{1.55}$/$BX_{0.84}$ and $GG_{1.55}$/$NC_{1.46}$/$BX_{0.84}$) was determined under different pH conditions (pH 4−9), as depicted in Figure 3b. The hydrogels reached their swelling equilibrium within 6 h. Under alkaline conditions, a substantial increase in the SI was observed upon addition of NC to the $GG_{1.55}$/$BX_{0.84}$-based hydrogel, as it provides mechanical strength to the hydrogel due to stronger H-bonding between the constituents in aqueous solution. This is due to the fact that in acidic conditions, cross-linked networking was unable to efficiently ionize, keeping the hydrogels in a less flexible, collapsed state. In contrast, alkaline conditions provide increased hydrogen bonding that led to the development of more cross-linked chains. The increased water intake by cross-linked hydrogel at higher pH might be attributed to the antagonistic interactions between the anionic component of the alkaline buffer and negatively charged $B(OH)^{4-}$ ions, which further induces intranetwork voids to expand even more to retain maximum amount of water, thereby enabling excellent MB carrying capacity of hydrogel.[15]

GF (%) was determined to check the cross-linkage between $B(OH)^{4-}$ and the −OH groups of GG and NC. Under neutral pH, the $GG_{1.55}$/$BX_{0.84}$ hydrogel showed 85.0%, whereas $GG_{1.55}$/$NC_{1.46}$/$BX_{0.84}$ revealed 95.2% of GF % value. This increased value of GF % resulted from large amounts of $B(OH)^{4-}$ ions interacting with −OH groups of biopolymer constituents of hydrogels. Additionally at a higher pH, GF % value was found to be higher in BX-based hydrogels that corresponds to the stronger cross-linking of BX at higher pH values.[33] Another finding also indicated that the high GF of hydrogels resulted from the higher degree of cross-linking in the polymer network.[34]

3.3.2. BET Analysis. The surface chemistry of the adsorbent exerts a major effect on the adsorption process. In the present study, the specific surface area of $GG_{1.55}$/$NC_{1.46}$/$BX_{0.84}$ (8.309 $m^2\ g^{-1}$) was found to be significantly higher than that of $GG_{1.55}$/$BX_{0.84}$ (7.676 $m^2\ g^{-1}$). This increased surface area of $GG_{1.55}$/$NC_{1.46}$/$BX_{0.84}$ might be attributed to the higher surface area and smaller particle size of NC. The mesoporous nature of

https://doi.org/10.1021/acsomega.3c06924
ACS Omega 2024, 9, 8904−8922

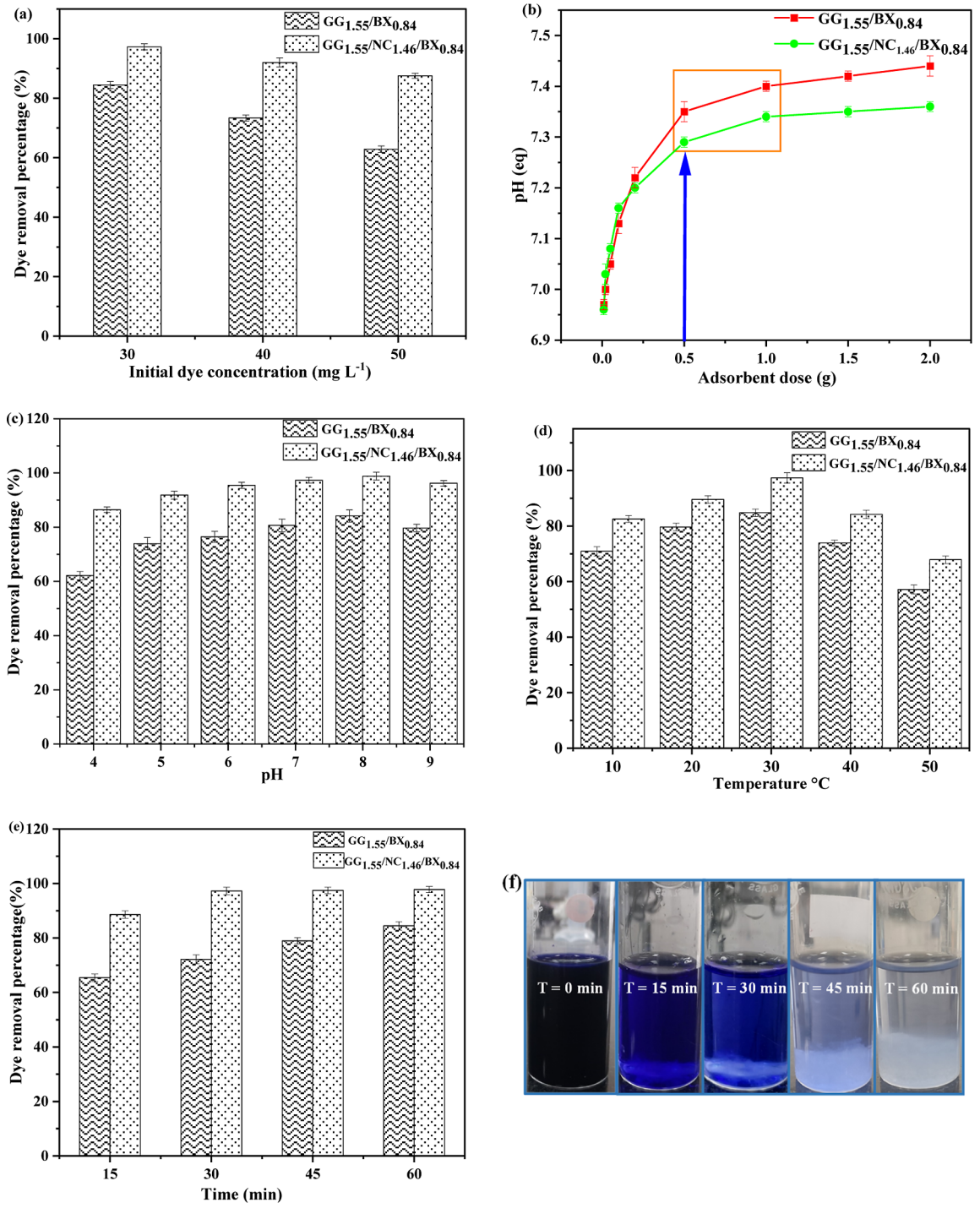

Figure 5. (a) Dye removal percentage at different initial dye concentrations, (b) point-of-zero-charge (Pzc), (c) dye removal percentage at different pHs, (d) dye removal percentage at different temperatures, I dye removal percentage at different times, and (f) images of dye adsorption at different contact times of $GG_{1.55}/BX_{0.84}$ and $GG_{1.55}/NC_{1.46}/BX_{0.84}$ hydrogels.

both hydrogels was demonstrated by type IV isotherm with H3 hysteresis loop (Figure S2), which means that a maximum degree of adsorption happens before the saturation pressure is reached. An adsorbent with a higher surface area has smaller pores. An adsorbent with a higher surface area has smaller pores, which exhibits a higher q_e.[29] Hence, it is worth mentioning here that the average pore size of $GG_{1.55}/NC_{1.46}/BX_{0.84}$ hydrogel was found to be smaller (1.939 nm) than that of $GG_{1.55}/BX_{0.84}$ hydrogel (3.412 nm), demonstrating higher q_e of the NC-incorporated hydrogel. Further, 0.011 $cm^3\ g^{-1}$ value of total pore volume was found in the case of $GG_{1.55}/BX_{0.84}$, whereas 0.012 $cm^3\ g^{-1}$ of total pore volume was obtained in the case of $GG_{1.55}/NC_{1.46}/BX_{0.84}$.

3.3.3. Biodegradability. Following a biodegradability test in soil, the weight loss (%) of the two hydrogels was estimated (Figure 3c). It is important to note that the addition of NC in the hydrogel ($GG_{1.55}/NC_{1.46}/BX_{0.84}$) resulted in a considerably lower rate of weight loss than the $GG_{1.55}/BX_{0.84}$ hydrogel. Upon addition of optimal NC concentration, the weight loss in the $GG_{1.55}/BX_{0.84}$ hydrogel dropped from 98.24 to 47.04% on

https://doi.org/10.1021/acsomega.3c06924
ACS Omega 2024, 9, 8904−8922

the third day. However, 98.72% of weight loss was observed in NC-incorporated hydrogel on the seventh day (Figure 3d). A significant reduction in weight loss (%) may have been as a result of the smaller pore size of NC-incorporated hydrogel, which inhibits soil microbes from entering the swollen hydrogel.[4]

3.3.4. Recyclability. The recyclability of hydrogel samples was demonstrated by the percentage removal of MB dye through adsorption−desorption cycles. It has been observed that the $GG_{1.55}/BX_{0.84}$ hydrogel was reused twice with a maximum dye removal capacity of 43.6%, whereas $GG_{1.55}/NC_{1.46}/BX_{0.84}$ exhibited 64.58% dye removal efficiency even after it was used for 4 consecutive cycles (Figure 3e). The $GG_{1.55}/BX_{0.84}$ hydrogel degraded prior to $GG_{1.55}/NC_{1.46}/BX_{0.84}$ due to its mechanically less resilient structure that leads to earlier degradation of polymer chains in $GG_{1.55}/BX_{0.84}$ hydrogel on repeated alkali treatment.[4] The current investigations were found to be in better agreement with earlier studies, where the CMC-Alg/GO hydrogel beads exhibited 76.07% of MB dye removal efficiency,[35] and the cellulose nanocrystals hydrogel (CNCsH) showed only 35% of AR8 dye removal efficiency[4] even after 4 successive adsorption−desorption cycles. Dynamic light scattering (DLS) analysis was performed on hydrogels after each cycle of reuse, revealing a consistent reduction in particle size of hydrogels after every reuse cycle (Figure 3f). This might be attributed to the repeated cycles of swelling and deswelling which subjected the hydrogel structure to mechanical stress and shear forces. These forces may lead to the fragmentation of the hydrogel particles, resulting in smaller and more dispersed particles.

3.4. Adsorption Studies for the Removal of MB Dye.

3.4.1. Adsorption Mechanism. During adsorption, the MB dye gets adsorbed on the surface of the $[B(OH)_4]^-$-intercalated GG/NC-based hydrogel. MB dye has cationic imine and amine groups by which it gets adsorbed on the cross-linked hydrogel. The adsorption of MB dye on the $[B(OH)_4]$-cross-linked hydrogel is facilitated by various electrostatic interactions such as electrostatic attraction (green hyphen) between the positively (+) charged imine nitrogen of the MB dye and the negatively (−) charged hydroxyl groups of the hydrogel as well as H-bonding interactions (red hyphen) between the amine group of the MB dye and the −OH group of the hydrogel composite (Figure 4a,b).

3.4.2. Effect of Initial Dye Concentration on MB Adsorption. To ascertain the impact of the initial dye concentration (30−50 mg L^{-1}) on the adsorption rate, kinetic studies were carried out on both hydrogels (Figure 5a).[15] The maximum *R* % was found to be 84.45 and 97.29%, respectively, for $GG_{1.55}/BX_{0.84}$ and $GG_{1.55}/NC_{1.46}/BX_{0.84}$ at 30 mg L^{-1} and pH 7 due to the high driving force of dye molecule relocation at the initial concentration of MB. On the contrary, the decline in *R* % was noticed from 73.36 to 62.86% for $GG_{1.55}/BX_{0.84}$ and from 92.03 to 87.53% for $GG_{1.55}/NC_{1.46}/BX_{0.84}$ as the initial dye concentration increased from 40 to 50 mg L^{-1}, respectively. This might be due to the saturation of adsorption sites on the hydrogel surface due to the deposition of dye molecules at the hydrogel interface. Further, due to the competition for the remaining active adsorption sites on the adsorbent, the electrostatic repulsion between dye molecules increased with increasing dye concentration, which led to a decrease in *R* %. In a recent investigation of a NC-based hydrogel, similar electrostatic repulsion between AR8 dye molecules and the adsorbent surface was observed upon increase of the dye concentration (10−30 ppm).[4] Hence, it is worth mentioning that the rate of adsorption affected by the type of dye, dye concentration, and more importantly the composition of the adsorbent.

3.4.3. Effect of pH on MB Adsorption. The efficacy of adsorption is substantially influenced by the pH of the solution that affects the charge on the cross-linked hydrogel and MB dye surface. The surface charge distribution of $GG_{1.55}/BX_{0.84}$ and $GG_{1.55}/NC_{1.46}/BX_{0.84}$ was examined by measuring the point-of-zero-charge (Pzc) in accordance with a previously described method.[36] At pH < Pzc, hydrogels would be positively charged, whereas at pH > Pzc hydrogels remain negatively charged. In cases of $GG_{1.55}/BX_{0.84}$ and $GG_{1.55}/NC_{1.46}/BX_{0.84}$, Pzc was found to be at pH 7.35 and 7.29, respectively (Figure 5b). Therefore, the adsorption of MB dye by $GG_{1.55}/BX_{0.84}$ and $GG_{1.55}/NC_{1.46}/BX_{0.84}$ would be more effective at pH > 7.35 and 7.29, respectively, as adsorbents would have more negative surface charge for the positively charged dimethylamine groups. At low pH, the surface charge becomes more positive that leads to the electrostatic repulsion between the hydrogel surface and positively charged dimethylamine groups of dye. Further, previous findings suggest that at pH > 6 the positively charged dimethylamine groups become more prominent.[19,37] In the current study, the impact of pH (4−9) on MB dye adsorption was investigated (Figure 5c), whereas in cases of $GG_{1.55}/BX_{0.84}$ and $GG_{1.55}/NC_{1.46}/BX_{0.84}$ hydrogels, the *R* % value gradually increased upon increasing the pH from 4 to 8. The $GG_{1.55}/BX_{0.84}$ and $GG_{1.55}/NC_{1.46}/BX_{0.84}$ hydrogels exhibited maximum adsorption at pH 8 with the maximum *R* % of 84.12 and 98.8%, respectively, which may be attributed to the higher electrostatic interactions between MB dye molecules and −OH groups on the hydrogel surface. In some previous studies, maximum adsorption of MB ions was also noticed on the adsorbent surface in alkaline conditions due to the presence of protonated MB dimethyl amine molecules and vice versa.[19,38]

3.4.4. Effect of Temperature on MB Adsorption. The temperature dependence of MB adsorption onto the hydrogel surface was studied within the temperature range of 10−50 °C and dye concentration of 30 mg L^{-1} at pH 7. Figure 5d illustrates a noticeable rise in *R* % value as the temperature increased within 10−30 °C from 70.94 ± 1.63 to 84.78 ± 1.35 and from 82.55 ± 1.23 to 97.33 ± 1.84% in cases of $GG_{1.55}/BX_{0.84}$ and $GG_{1.55}/NC_{1.46}/BX_{0.84}$, respectively. This phenomenon can be attributed to the initial heat supplied, which serves as the activation energy, driving this upward trend. However, beyond 30 °C, a decline in *R* % value was observed as the temperature increased from 30 to 50 °C in the case of both hydrogels (for $GG_{1.55}/BX_{0.84}$, from 84.78 ± 1.35 to 57.16 ± 1.66% and for $GG_{1.55}/NC_{1.46}/BX_{0.84}$ from 97.33 ± 1.84 to 67.05 ± 1.39%). As already mentioned, at high temperatures, the SI reduced that ultimately led to a decrease in the *R* % value due to the unavailability of active adsorption sites on the hydrogel surface, as well as a decline in quality transportation of the MB dye molecules on the hydrogel surface. In the present scenario, the *R* % decreased above 30 °C as the available active sites are fully occupied and therefore 30 °C is considered an ideal temperature for MB dye removal. Similar results were reported for the q_e of AR8 by CNCsH[4] and MB dye by the cross-linked PAA-based hydrogel.[13]

3.4.5. Effect of Contact Time on MB Adsorption. The effect of contact time (15−60 min) on adsorbate adsorption was examined as shown in Figure 5e,f. With increasing contact

https://doi.org/10.1021/acsomega.3c06924
ACS Omega 2024, 9, 8904−8922

Table 5. Kinetic Model Parameters for MB Dye Removal by $GG_{1.55}/BX_{0.84}$ and $GG_{1.55}/NC_{1.46}/BX_{0.84}$[a]

	$GG_{1.55}/BX_{0.84}$						$GG_{1.55}/NC_{1.46}/BX_{0.84}$					
	pseudo-first-order			pseudo-second-order			pseudo-first-order			pseudo-second-order		
initial dye conc. (C_0) (mg L^{-1})	q_e (mg g^{-1})	k_1 (min^{-1})	R^2	q_e (mg g^{-1})	k_2 (g mg^{-1} min)	R^2	q_e (mg g^{-1})	k_1 (min^{-1})	R^2	q_e (mg g^{-1})	k_2 (g mg^{-1} min)	R^2
30	13.17	0.0181	0.4849	13.17	0.02	0.9996	12.60	0.130	0.8052	12.60	0.0390	1.0000
40	17.47	0.204	0.8948	17.47	0.09	0.9998	15.48	0.140	0.7838	15.48	0.0318	0.9995
50	21.85	0.220	0.0642	21.85	0.05	0.9978	24.59	0.161	0.8242	24.59	0.0329	0.9983

[a]Adsorbent amount = 0.02 g, pH = 8, time = 30 min, and temperature = 30 °C.

Table 6. Different Parameters of Isotherm Models for MB Dye Removal by $GG_{1.55}/BX_{0.84}$ and $GG_{1.55}/NC_{1.46}/BX_{0.84}$

	Langmuir				Freundlich		
model	q_m	K_L	R_L	R^2	$1/n_f$	K_F	R^2
$GG_{1.55}/BX_{0.84}$	44.64	0.119	0.143	0.9521	0.678	5.8	0.9566
$GG_{1.55}/NC_{1.46}/BX_{0.84}$	126.58	0.0453	0.306	0.8172	0.367	5.54	0.9889

time, a high slope of curve obtained initially demonstrating a high R % value and after that slowly approaches a much lower sorption rate. This indicated that the adsorption reaction perhaps occurred in two different phases: where initially MB dye was removed by rapid external surface adsorption, followed by transportation of surface-adsorbed MB dye to the internal adsorption sites of the hydrogel. Parallel results have been reported in previous study of AO7 dye removal by gel-anion exchangers, where saturation in dye adsorption was achieved within 10 min at initial dye concentration.[39] In the present study, $GG_{1.55}/BX_{0.84}$ and $GG_{1.55}/NC_{1.46}/BX_{0.84}$ showed maximum MB dye adsorption within 60 and 30 min, respectively, indicating the achievement of equilibrium because of the unavailability of active adsorption sites. The higher adsorption rate in the case of $GG_{1.55}/NC_{1.46}/BX_{0.84}$ might be due to the high surface area and higher number of active adsorption sites, which subsequently resulted in stronger electrostatic attraction between the charged moieties of MB dye and the hydrogel surface causing equilibrium to reach within a shorter contact time. In Figure S3, the time-dependent UV−vis spectra of MB dye after it was adsorbed on the hydrogel surface demonstrated a notable hypochromic shift at 580 nm. This shift is indicative of the aggregation of the MB dye molecules, suggesting the formation of MB dye dimers.

3.4.6. Adsorption Kinetics. The adsorption mechanism and rate-controlling steps for MB dye adsorption on hydrogel can be revealed through kinetic investigations. The kinetic models, including the linear form of pseudo-first-order (eq 11) and pseudo-second order (eq 12), were used to analyze the adsorption kinetics of MB dye onto $GG_{1.55}/BX_{0.84}$ and $GG_{1.55}/NC_{1.46}/BX_{0.84}$ hydrogels.

$$\log(q_e - q_t) = \log q_e - \frac{k_1 t}{2.303} \tag{11}$$

$$\frac{t}{q_t} = \frac{1}{k_2 q_e^2} + \frac{t}{q_e} \tag{12}$$

where q_e (mg g^{-1}) is the adsorption capacity at equilibrium time and q_t (mg g^{-1}) is the adsorption capacity at time t (min). k_1 (min^{-1}) and k_2 (g mg^{-1} min^{-1}) are the rate constants of pseudo-first-order and pseudo-second-order reactions, respectively. To assess all related parameters and experimental results, the slope and intercepts of linear plots of $\log(q_e - q_t)$ versus t and t/q_t versus t were used for pseudo-first-order and pseudo-second-order reactions, respectively (Table 5 and Figure S4).

In both cases ($GG_{1.55}/BX_{0.84}$ and $GG_{1.55}/NC_{1.46}/BX_{0.84}$), the kinetic profile of the MB adsorption process is better suggested by the high degree of linearity of the pseudo-second-order model. The greater correlation coefficient (R^2) of the pseudo-second-order model can better describe the MB adsorption behavior of hydrogels as compared to that of pseudo-first-order. The superior fit of pseudo-second-order model by both hydrogels indicates that the overall adsorption rate is driven by the electrostatic interactions and hydrogen bonds between the hydrogel and MB. These findings support the experimental results obtained from the effect of pH study.

3.4.7. Adsorption Isotherm. Adsorption isotherm is essentially important as it describes how the adsorbate and adsorbent interact with each other. The isothermal behavior of the adsorption process by resulting hydrogels was described by two isotherm adsorption models, i.e., Langmuir and Freundlich. The Langmuir model is given by eq 13:

$$\frac{C_e}{q_e} = \frac{1}{K_L q_m} + \frac{C_e}{q_m} \tag{13}$$

where C_e (mg L^{-1}) is the concentration of dye in solution at equilibrium, q_e (mg g^{-1}) is the adsorption capacity at equilibrium, q_m (mg g^{-1}) is the maximum adsorption capacity, and K_L (L mg^{-1}) is a Langmuir adsorption constant at equilibrium. The Langmuir isotherm can express a dimensionless constant (R_L) called the balance parameter or separation factor (eq 14):

$$R_L = \frac{1}{1 + K_L C_0} \tag{14}$$

The Freundlich model is given by eq 15:

$$\log q_e = \log K_F - \frac{1}{n} \log C_e \tag{15}$$

where K_F is the empirical constant related to the maximum adsorption quantity and n is the empirical constant related to adsorption intensity.

Table 6 represents the calculated parameters of the studied isothermal models. The correlation coefficients (R^2) of 0.9521 ($GG_{1.55}/BX_{0.84}$) and 0.8172 ($GG_{1.55}/NC_{1.46}/BX_{0.84}$) for the Langmuir model and 0.9566 ($GG_{1.55}/BX_{0.84}$) and 0.9889 ($GG_{1.55}/NC_{1.46}/BX_{0.84}$) for the Freundlich model indicate that

https://doi.org/10.1021/acsomega.3c06924
ACS Omega 2024, 9, 8904−8922

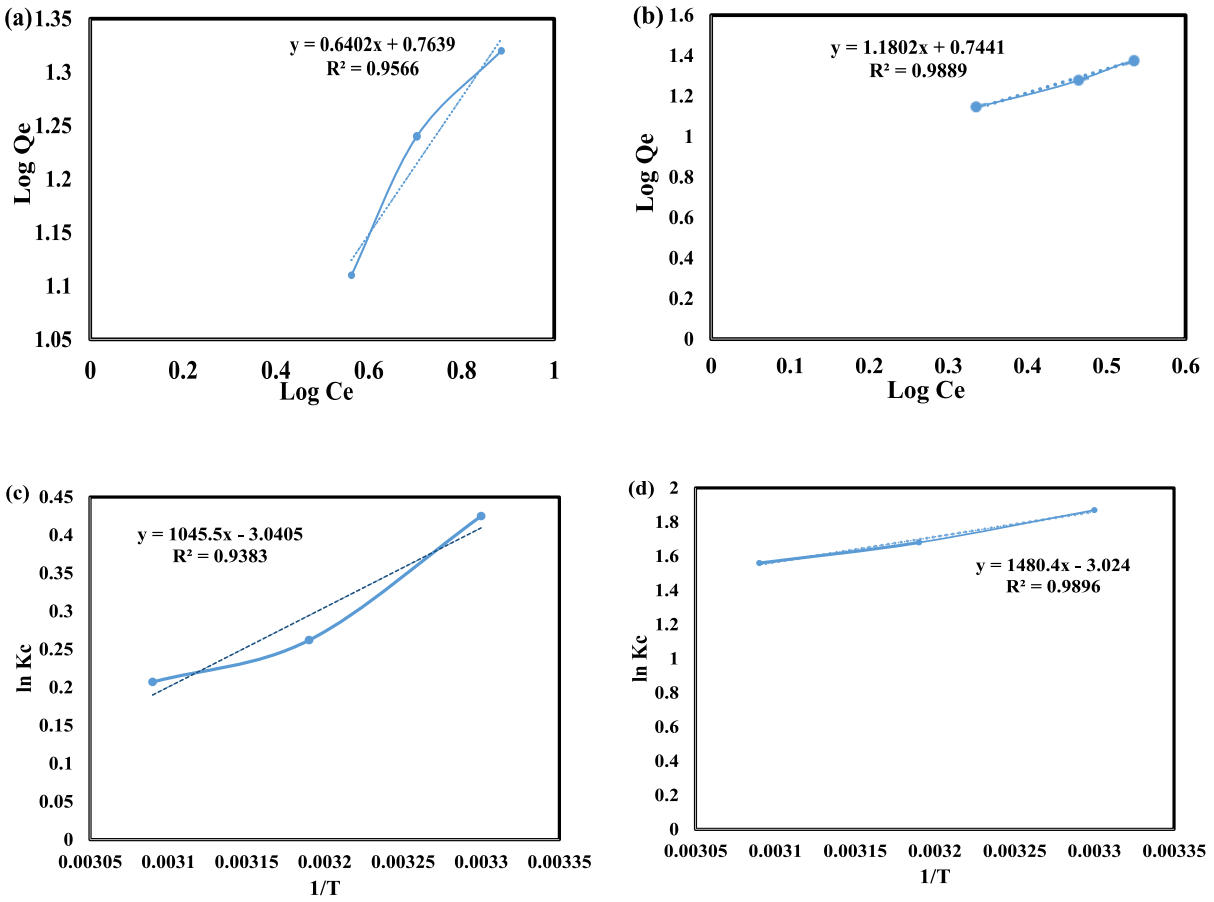

Figure 6. Graphs of isotherm models: (a,b) Freundlich model and (c,d) thermodynamic studies (classic van't Hoff plot) for MB adsorption on $GG_{1.55}/BX_{0.84}$ and by $GG_{1.55}/NC_{1.46}/BX_{0.84}$.

the adsorption behavior of hydrogels is more consistent with the Freundlich adsorption model. Per Freundlich adsorption model, the adsorption is independent of pressure when $1/n = 0$ and x/m is constant, whereas adsorption is directly proportional to pressure when $1/n = 1$ and $x/m = kP$, i.e., $x/m \propto P$. Figure 6a,b demonstrates the plots of log q_e versus log C_e for $GG_{1.55}/BX_{0.84}$ and $GG_{1.55}/NC_{1.46}/BX_{0.84}$. The present adsorption study revealed that the MB dye can be adsorbed inside the hydrogel for high-concentration adsorption at different localized adsorption sites on hydrogel (multiple-layer adsorption). Hence, it can be concluded that during dye diffusion with hydrogel, more MB penetrated inside of the hydrogel as compared to the surface adsorption. Similar findings were reported in previous research work, where the CNC-β-CD/α-CD/Pluronic F127 hydrogel (CCH) was modified by grafting acrylic acid to form the acrylated composite hydrogel (ACH) for the adsorption of MB dye.[40]

3.4.8. Thermodynamic Studies of Adsorption. To determine the thermodynamic feasibility, spontaneity, and the impact of temperature on adsorption, thermodynamic parameters like Gibbs free energy change (ΔG, mol^{-1}), enthalpy change (ΔH, kJ mol^{-1}), and entropy change (ΔS, J mol^{-1} K^{-1}) were calculated using eqs 16−19, respectively:

$$\Delta G^\circ = -RT \ln K_c \tag{16}$$

$$\ln K_c = \frac{C_{ads}}{C_e} \tag{17}$$

$$\ln K_c = \frac{\Delta S^\circ}{R} - \frac{\Delta H^\circ}{RT} \tag{18}$$

$$\Delta G^\circ = \Delta H^\circ - T\Delta S^\circ \tag{19}$$

where K_c is the thermodynamic constant, C_{ads} and C_e are the equilibrium concentrations of MB (mg g^{-1}) on the nanocomposite and solution (mg L^{-1}), respectively, R is the universal gas constant (8.314 mol K^{-1}), and T is the absolute temperature of solution (K). The values of ΔH° and ΔS° were determined based on the slope and intercept of classic van't Hoff plot of ln K_c versus $1/T$ (Table 7).[16]

Adsorption of MB on hydrogels decreased as the temperature increased from 30 to 50 °C, as shown in Figure 5d,e. Table 7 demonstrates all the thermodynamic parameters, from which the slope and the intercept of the ln K_c versus $1/T$ plot (Figure 6c,d) were used to determine the values of enthalpy change (ΔH°) and entropy change (ΔS°). In the present

Table 7. Thermodynamic Parameters of MB Dye Adsorption on $GG_{1.55}/BX_{0.84}$ and $GG_{1.55}/NC_{1.46}/BX_{0.84}$

thermodynamic parameters	$GG_{1.55}/BX_{0.84}$	$GG_{1.55}/NC_{1.46}/BX_{0.84}$
ΔS° (J mol^{-1} K^{-1})	−0.025	−0.025
ΔH° (kJ mol^{-1})	−8.692	−12.30
ΔG° (kJ mol^{-1})		
30 °C	−16.17	−4.71
40 °C	−16.42	−4.37
50 °C	−16.67	−4.18

https://doi.org/10.1021/acsomega.3c06924
ACS Omega 2024, 9, 8904−8922

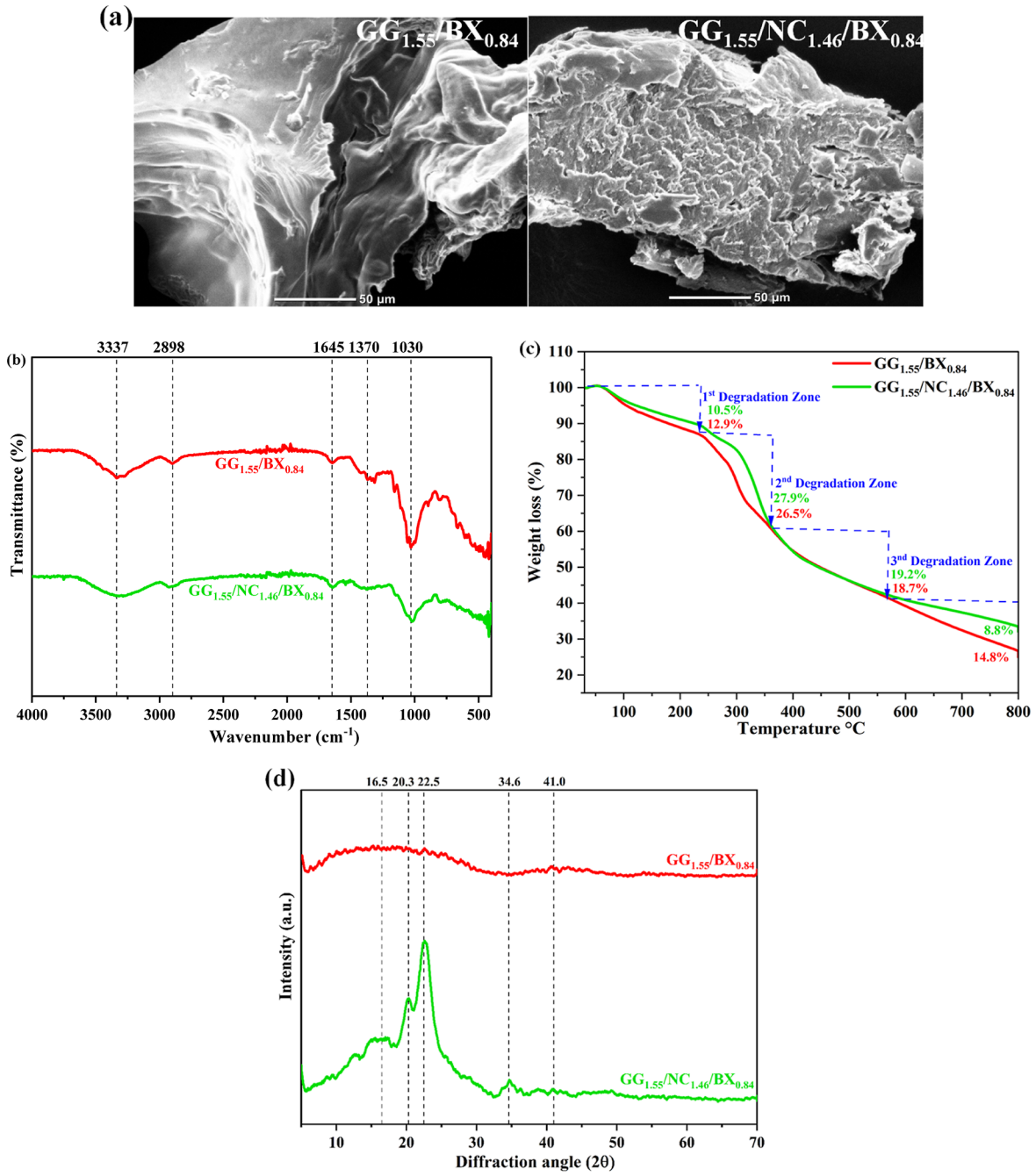

Figure 7. (a) SEM micrograph, (b) FTIR spectra, (c) TGA graph, and (d) XRD spectra of $GG_{1.55}/BX_{0.84}$ and $GG_{1.55}/NC_{1.46}/BX_{0.84}$ hydrogels.

study, the negative values of ΔH° suggest that the nature of adsorption was exothermic, confirmed by the weak interaction between the dye molecules and the hydrogel surface in both cases. Hence, in both cases, adsorption processes were complex physicochemical processes. The Gibbs free energy (ΔG°) demonstrated that the adsorption process indications decrease in Gibbs energy, therefore, revealed that the adsorption processes are feasible and spontaneous in nature.[41] Likewise, the negative value of ΔS° has established the decrease of randomness at the solid/liquid interface during the adsorption process. Hence, thermodynamic parameters corresponding to the present hydrogel specified that the adsorption process can be used for the removal of the MB dye pollutant. Parallel findings have been reported for another NC-based hydrogel used for the removal of AR8 dye.[4]

3.5. Characterization. *3.5.1. Morphological Study.* The surface morphologies of cross-linked $GG_{1.55}/BX_{0.84}$ and $GG_{1.55}/NC_{1.46}/BX_{0.84}$ hydrogels were examined using SEM (Figure 7a). The morphology of the BX cross-linked GG hydrogel changed noticeably upon NC incorporation. At 50 μm resolution, a significant change with a narrow pore network structure was observed in the NC-incorporated hydrogel as compared to the $GG_{1.55}/BX_{0.84}$ hydrogel, where a slightly less porous structure was observed. The complete dispersion and anchoring of NC nanoparticles on the hydrogel surface correspond to the occurrence of more cross-links between −OH groups of NC induced by BX. These outcomes might lead to the generation of a noticeable interconnected porous structure of $GG_{1.55}/NC_{1.46}/BX_{0.84}$. Similar outcomes of

https://doi.org/10.1021/acsomega.3c06924
ACS Omega 2024, 9, 8904−8922

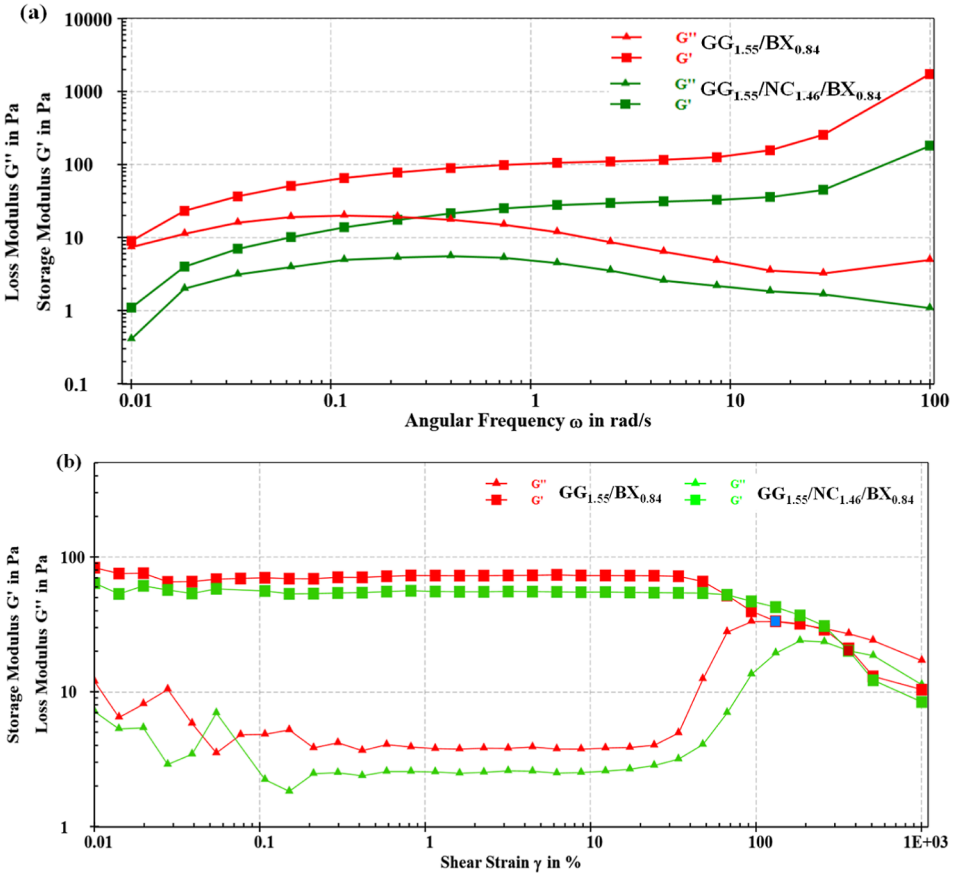

Figure 8. Rheological analysis: (a) frequency sweep and (b) strain sweep of $GG_{1.55}/BX_{0.84}$ and $GG_{1.55}/NC_{1.46}/BX_{0.84}$ hydrogels.

cellulose-derived porous hydrogels were witnessed for the present findings.[4,26]

3.5.2. FTIR-ATR Analysis. The FTIR spectra confirmed the chemical modifications of hydrogels (Figure 7b). In both cases, the broad absorption band between 3600 and 3000 cm^{-1} was related to O−H stretching vibrations. However, a more pronounced band with a slight shift from 3343 cm^{-1} ($GG_{1.55}/BX_{0.84}$) to 3337 cm^{-1} ($GG_{1.55}/NC_{1.46}/BX_{0.84}$) was observed in the case of NC-incorporated hydrogel that can be inferred from the appearance of new H-bonded O−H structures. The peaks observed at around 2930−2850 cm^{-1} were related to C−H stretching vibrations of the CH_2 group from the polymer backbone, whereas peaks between 1640 and 1650 cm^{-1} corresponded to O−H bending vibrations related to ring stretching vibrations and associated water molecules.[12,17] Additionally, a slight shift of the absorption band at 1647 cm^{-1} ($GG_{1.55}/BX_{0.84}$) to 1645 cm^{-1} ($GG_{1.55}/NC_{1.46}/BX_{0.84}$) confirms the formation of stronger inter-/intramolecule hydrogen bonding between components of the $GG_{1.55}/NC_{1.46}/BX_{0.84}$ hydrogel.[42] Upon addition of BX, the FTIR spectra of both hydrogels showed typical peaks of BX and borate around 1370 cm^{-1}, attributed to the asymmetric stretching relaxation of the didiol complex. Such peaks indicated the cross-linking network between −OH groups of biopolymer components and borate ions, as also described in the earlier study.[26] The NC-incorporated hydrogel represented an arrangement of some additional main peaks at around 1400 cm^{-1} (C−H bending), 1160 cm^{-1} (C−O−C stretching), and 894 cm^{-1} (β-1,4 glycosidic linkage), suggesting the successful incorporation of NC in the hydrogel composite.[12]

3.5.3. Thermal Analysis. TGA was performed to determine the thermal stability of the hydrogel composite (Figure 7c). Three different zones of weight loss were obtained in each case. The first decomposition zone (30−230 °C) was related to the weight loss due to the moisture content, where in cases of $GG_{1.55}/BX_{0.84}$ and $GG_{1.55}/NC_{1.46}/BX_{0.84}$, 12.9 and 10.5% of weight loss occurred, respectively. The second decomposition zone (230−350 °C) was associated with the weight loss of 26.5% ($GG_{1.55}/BX_{0.84}$) and 27.9% ($GG_{1.55}/NC_{1.46}/BX_{0.84}$), attributed to the degradation of the polysaccharide backbone of $GG_{1.55}/BX_{0.84}$. The third decomposition zone (350−550 °C), represented the breakdown of the cross-linked bonds between borate ions of BX and −OH groups of the biopolymer components of the hydrogel, where around 18.7 and 19.2% weight loss occurred in both cases, respectively. Finally, regarding the total combustion of the residual weight at around 550−800 °C, described as char, the $GG_{1.55}/NC_{1.46}/BX_{0.84}$ hydrogel exhibited lesser weight loss (8.8%) as compared to $GG_{1.55}/BX_{0.84}$ (14.8%), indicating higher thermal stability of the NC-incorporated hydrogel. Similar outcomes related to GG-based hydrogel have also been reported in previous studies.[43,44]

3.5.4. XRD Analysis. Structural evolution, especially the crystallinity of resultant hydrogels, was effectively analyzed by XRD, as shown in Figure 7d. The amorphous phase of GG in the case of $GG_{1.55}/BX_{0.84}$ hydrogel was represented by a broad hump between the scattering angles of 10−40°, demonstrating the development of cross-linked GG, as also reported in previous studies.[19,45,46] Compared to $GG_{1.55}/BX_{0.84}$, the $GG_{1.55}/NC_{1.46}/BX_{0.84}$ hydrogel exhibited different XRD

https://doi.org/10.1021/acsomega.3c06924
ACS Omega 2024, 9, 8904−8922

Table 8. Comparison Study of the $GG_{1.55}/NC_{1.46}/BX_{0.84}$ Hydrogel Composite for the Removal of Dyes with Previously Reported GG- and NC-Based Hydrogels

adsorbent	dye	SI (%)	q_e (mg g^{-1})	R (%)	reusability (cycles)	ref
GG-*g*-acrylamide	AR8	1400	18		3	17
CNCsH	AR8	2770	17.12		4	4
(PMPC/BNC)	MB and methyl orange	627−912	4.4−4.5			24
GG-cl-poly(acrylic acid)	MB	2345.06		93.867		50
poly(acrylic acid−acrylamide)	crystal violet		4.12			51
poly(acrylic acid−acrylamide)	basic magenta		11.23			51
CT hydrogel	MB		0.40	80	6	23
$GG_{1.55}/NC_{1.46}/BX_{0.84}$	MB	3741.42	24.05		4	present CIAB work

patterns with sharper and significant peaks at 16.5, 22.5, and 34.6°, attributed to the successful NC grafting and ultimately the higher crystallinity. The crystalline structure of the NC-incorporated hydrogel was probably the consequence of significant intramolecular and intermolecular H-bonds formed by polymer chains, or the polymer chains and NC. The major peaks in $GG_{1.55}/NC_{1.46}/BX_{0.84}$ at around 20.5 and 41.0° were assigned to GG.[44,46] It is worth mentioning that the amorphous structure of the $GG_{1.55}/BX_{0.84}$ hydrogel was resolved because of NC addition. Higher crystallinity might signify the higher mechanical strength of NC-incorporated hydrogel because of resilient inter-/intermolecular bonding between hydrogel constituents.

3.6. Rheological Studies. Oscillatory rheology analyses were carried out to investigate the viscoelastic and mechanical properties of the freshly prepared hydrogel composite (Figure 8). In the frequency-dependent oscillatory rheology test (Figure 8a), the elastic modulus G' was found to be greater than the viscous modulus G'', representing elasticity-dominant properties in both hydrogels. The considerable increase of the storage or elastic modulus (G'), irrespective of the frequency (0.01−100 rad s^{-1}), clearly indicates the gel-like behavior of $GG_{1.55}/BX_{0.84}$ and $GG_{1.55}/NC_{1.46}/BX_{0.84}$ hydrogels. In addition, no crossover points were observed over the entire range of frequency in both hydrogels. Gels always produced at above critical cross-linking concentration (c^*) of the cross-linker.[47] Thus, the clear independence of G' over the entire range of frequency at the optimized concentration of BX (0.84%) demonstrates the gel-like behavior of both hydrogels.

It has been clearly noticed from strain-dependent oscillatory rheology (Figure 8b) that the G' of both hydrogels is independent of strain (γ) up to a broad range, which is known as LER. A particular stress (τ) at which G' unexpectedly decreases is considered the yield stress (τ^*) of the hydrogel. In the current study (Figure 8b), at the flow point (crossover points of G' and G''), higher stress (τ = 104.1 Pa) and strain (γ = 362.5%) were observed in the case of $GG_{1.55}/NC_{1.46}/BX_{0.84}$ hydrogel in contrast to the $GG_{1.55}/BX_{0.84}$ hydrogel (τ = 62.28 Pa and γ = 131.3%), which confirmed the improvement in mechanical properties of hydrogel due to the NC incorporation.[48] This might be due to the higher surface area of the composite, as mentioned in BET analysis of the hydrogel. The present observations revealed the importance of NC addition in the hydrogel as it provides a high surface area and more active sites to easily interact with GG and BX, eventually enhancing the gel strength to withstand greater external forces without failure.[49]

3.6.1. Relevance of the Present Research Work, Its Novelty, Recyclability, and Comparison with Literature Data. A comparison of the SI and adsorption capacities of the current $GG_{1.55}/NC_{1.46}/BX_{0.84}$ hydrogel was demonstrated with the previously reported studies related to GG- and NC-based hydrogels in Table 8. In a recent study, the GG-grafted acrylamide (GG-*g*-acrylamide) hydrogel was reported with an SI of 1400% to remove the acid red dye. A study demonstrated a hydrogel with 18 mg g^{-1} of dye q_e and 3 times recyclability upon increasing the grafting percentage of acrylamide.[17] Abdelaziz and their colleagues have reported an epichlorohydrin cross-linked crystalline NC (derived from office waste-paper)-based biodegradable hydrogel with an SI of 2770% for the removal of AR8 dye using 5% CNC concentration (q_e = 17.12 mg g^{-1} and R % = 68%) that showed 4 times recyclability.[4] Similarly, Vilela and their team have studied cross-linked PMPC/BNC for the removal of MB and methyl orange dye. They have stated that BNC 3D porous network incorporation demonstrated high thermal stability (250 °C), high SI (627−912%), and excellent mechanical property for the hydrogel.[24] Likewise, a tannin-immobilized cellulose (CT) hydrogel exhibited R % of 80% and q_e of 0.40 mg g^{-1} with 6 times recyclability.[23] In the present study, an innovative NC-based cross-linked hydrogel in combination with GG was investigated that provided a higher SI of 3241.42%, q_e of 24.05 mg g^{-1}, and R % of 98.8% with 4 cycles of reusability. In addition to this, better mechanical behavior with higher stress (τ = 104.1 Pa) and strain (γ = 362.5%) values and a high surface area of 8.309 m^2 g^{-1} due to NC incorporation revealed its better and easy interaction with the dye molecules, making it an ideal choice as a biodegradable adsorbent for the removal of dye pollutant from wastewater.

The novelty and relevance of current research work highlights its superior physical properties that set it apart from the other hydrogels reported in the literature. In the present study, an advanced NC-based cross-linked hydrogel has been developed in combination with GG (matrix) and BX (cross-linker). NC works well as a filler for its comparatively higher mechanical strength. Although several hydrogels have been reported based individually on NC and GG, only a few combinations of NC- and GG-based hydrogels are available that are rarely being considered for the removal of dye pollutants. It has been noticed that the current hydrogel provides higher SI, q_e, and dye removal percentage than above-discussed previous hydrogels along with maximum number of recycles.

4. CONCLUSIONS

A highly effective method was developed and optimized to synthesize a NC-based hydrogel in combination with GG, which serves as an efficient adsorbent for the removal of MB dye. The hydrogel was characterized using SEM, XRD, FTIR, and TGA, confirming its structural, functional, as well as

https://doi.org/10.1021/acsomega.3c06924
ACS Omega 2024, 9, 8904−8922

thermal properties. The maximum q_e was observed at pH 8, with an initial dye concentration of 30 mg L^{-1}, a contact time of 30 min, and a temperature of 30 °C. The equilibrium data was best described by the Freundlich isotherm model, indicating favorable adsorption behavior. The synthesized nanocomposite showed excellent SI and q_e of 3741.42% and 24.05 mg g^{-1}, respectively, as compared to other reported adsorbents. The kinetic study discovered that the pseudo-second-order model provided the best fit for MB dye removal. The adsorption process was exothermic and spontaneous, leading to decreased randomness at the solid/liquid interface. Further, the adsorbent demonstrated better reusability, allowing for 4 consecutive cycles of dye removal, highlighting its potential application for wastewater treatment.

■ ASSOCIATED CONTENT

Supporting Information

The Supporting Information is available free of charge at https://pubs.acs.org/doi/10.1021/acsomega.3c06924.

Schematic presentation of BX-cross-linked GG/NC -based hydrogel; BET N_2 adsorption−desorption isotherm plots of $GG_{1.55}/BX_{0.83}$ and $GG_{1.55}/NC_{1.46}/BX_{0.84}$ hydrogels; time-dependent UV−vis spectra of MB dye after adsorption; kinetic graphs of pseudo-second-order model for $GG_{1.55}/BX_{0.84}$ and $GG_{1.55}/NC_{1.46}/BX_{0.84}$ hydrogels; and ANOVA of the SI of the prepared hydrogel using a quadratic model (PDF)

■ AUTHOR INFORMATION

Corresponding Authors

Saswata Goswami − *Chemical Engineering Division, Center of Innovative and Applied Bioprocessing, Mohali, Punjab 140306, India;* orcid.org/0000-0001-9126-0761; Email: saswata@ciab.res.in, saswatagoswami2015@gmail.com

Dipti Sareen − *Department of Biochemistry, Panjab University, Chandigarh 160014, India*; Email: diptsare@pu.ac.in

Authors

Harshdeep Rana − *Chemical Engineering Division, Center of Innovative and Applied Bioprocessing, Mohali, Punjab 140306, India; Department of Biochemistry, Panjab University, Chandigarh 160014, India;* orcid.org/0000-0002-5568-1232

Anamika − *Chemical Engineering Division, Center of Innovative and Applied Bioprocessing, Mohali, Punjab 140306, India*

Complete contact information is available at: https://pubs.acs.org/10.1021/acsomega.3c06924

Author Contributions

Harshdeep Rana: Investigation, Methodology, Software, Experimental execution, Formal analysis, Writing—original draft, and Manuscript revision and editing. Anamika: Experimental data acquisition and kinetic and thermodynamic studies. Dipti Sareen: Supervision and Manuscript review and editing. Saswata Goswami: Conceptualization, Experimental design, Supervision, Manuscript review and editing, Resources, and Funding acquisition.

Notes

The authors declare no competing financial interest.

■ ACKNOWLEDGMENTS

All authors are thankful to the Center of Innovative and Applied Bioprocessing (CIAB), Mohali, for providing access to their research facilities and infrastructure and to Panjab University, Chandigarh, for providing access to their instrumentation facilities.

■ ABBREVIATIONS

NC	nanocellulose
GG	guar gum
BX	borax
MB	methylene blue
GG/NC	guar gum/nanocellulose
PVA	poly(vinyl alcohol)
PLA	polylactic acid
PCL	polycaprolactone
PEG	polyethylene glycol
SI	swelling index
GF	gel fraction
DLS	dynamic light scattering
SEM	scanning electron microscopy
XRD	X-ray diffraction
FTIR	Fourier transform infrared
TGA	thermogravimetric analysis

■ REFERENCES

(1) Navin, P. K.; Mathur, M. Textile-Wastewater-Treatment-a-Critical-Review. *Int. J. Eng. Res. Technol.* **2018**, *6* (11), 1−7.

(2) Ghoniem, M. G.; Ali, F. A. M.; Abdulkhair, B. Y.; Elamin, M. R. A.; Alqahtani, A. M.; Rahali, S.; Ben Aissa, M. A. Highly Selective Removal of Cationic Dyes from Wastewater by MgO Nanorods. *Nanomaterials* **2022**, *12* (6), 1023−1114.

(3) Dutta, S.; Gupta, B.; Srivastava, S. K.; Gupta, A. K. Recent Advances on the Removal of Dyes from Wastewater Using Various Adsorbents: A Critical Review. *Mater. Adv.* **2021**, *2* (14), 4497−4531.

(4) Abdelaziz, R. M.; El-Maghraby, A.; Sadik, W. A. A.; El-Demerdash, A. G. M.; Fadl, E. A. Biodegradable Cellulose Nanocrystals Hydrogels for Removal of Acid Red 8 Dye from Aqueous Solutions. *Sci. Rep.* **2022**, *12* (1), 6424−6517.

(5) Dassanayake, R. S.; Acharya, S.; Abidi, N. Recent Advances in Biopolymer-Based Dye Removal Technologies. *Molecules* **2021**, *26* (15), 4697.

(6) Dai, L.; Zhang, L.; Wang, B.; Yang, B.; Khan, I.; Khan, A.; Ni, Y. Multifunctional Self-Assembling Hydrogel from Guar Gum. *Chem. Eng. J.* **2017**, *330* (May), 1044−1051.

(7) El Sayed, M. M. Production of Polymer Hydrogel Composites and Their Applications. *J. Polym. Environ.* **2023**, *31* (7), 2855−2879.

(8) Tran, H. D. N.; Park, K. D.; Ching, Y. C.; Huynh, C.; Nguyen, D. H. A Comprehensive Review on Polymeric Hydrogel and Its Composite: Matrices of Choice for Bone and Cartilage Tissue Engineering. *J. Ind. Eng. Chem.* **2020**, *89*, 58−82.

(9) Li, N.; Liu, C.; Chen, W. Facile Access to Guar Gum Based Supramolecular Hydrogels with Rapid Self-Healing Ability and Multistimuli Responsive Gel-Sol Transitions. *J. Agric. Food Chem.* **2019**, *67* (2), 746−752.

(10) Shin, M. K.; Spinks, G. M.; Shin, S. R.; Kim, S. I.; Kim, S. J. Nanocomposite Hydrogel with High Toughness for Bioactuators. *Adv. Mater.* **2009**, *21* (17), 1712−1715.

(11) Han, J.; Lei, T.; Wu, Q. Facile Preparation of Mouldable Polyvinyl Alcohol-Borax Hydrogels Reinforced by Well-Dispersed Cellulose Nanoparticles: Physical, Viscoelastic and Mechanical Properties. *Cellulose* **2013**, *20* (6), 2947−2958.

(12) Fan, Q.; Jiang, C.; Wang, W.; Bai, L.; Chen, H.; Yang, H.; Wei, D.; Yang, L. Eco-Friendly Extraction of Cellulose Nanocrystals from Grape Pomace and Construction of Self-Healing Nanocomposite Hydrogels. *Cellulose* **2020**, *27* (5), 2541−2553.

(13) Hu, X. S.; Liang, R.; Sun, G. Super-Adsorbent Hydrogel for Removal of Methylene Blue Dye from Aqueous Solution. *J. Mater. Chem. A* **2018**, *6* (36), 17612−17624.
(14) Yang, J.; Han, C. R.; Duan, J. F.; Xu, F.; Sun, R. C. Mechanical and Viscoelastic Properties of Cellulose Nanocrystals Reinforced Poly(Ethylene Glycol) Nanocomposite Hydrogels. *ACS Appl. Mater. Interfaces* **2013**, *5* (8), 3199−3207.
(15) Thombare, N.; Jha, U.; Mishra, S.; Siddiqui, M. Z. Borax Cross-Linked Guar Gum Hydrogels as Potential Adsorbents for Water Purification. *Carbohydr. Polym.* **2017**, *168*, 274−281.
(16) Gupta, V. K.; Agarwal, S.; Ahmad, R.; Mirza, A.; Mittal, J. Sequestration of Toxic Congo Red Dye from Aqueous Solution Using Ecofriendly Guar Gum/Activated Carbon Nanocomposite. *Int. J. Biol. Macromol.* **2020**, *158*, 1310−1318.
(17) Batouti, M. E.; Sadik, W.; Eldemerdash, A. G.; Hanafy, E.; Fetouh, H. A. New and Innovative Microwave-Assisted Technology for Synthesis of Guar Gum-Grafted Acrylamide Hydrogel Super-absorbent for the Removal of Acid Red 8 Dye from Industrial Wastewater. *Polym. Bull.* **2022**, *80*, 4965−4989.
(18) Hiremath, J. N.; Vishalakshi, B. Evaluation of a PH-Responsive Guar Gum-Based Hydrogel as Adsorbent for Cationic Dyes: Kinetic and Modelling Study. *Polym. Bull.* **2015**, *72* (12), 3063−3081.
(19) Santoso, S. P.; Angkawijaya, A. E.; Bundjaja, V.; Hsieh, C. W.; Go, A. W.; Yuliana, M.; Hsu, H. Y.; Tran-Nguyen, P. L.; Soetaredjo, F. E.; Ismadji, S. TiO2/Guar Gum Hydrogel Composite for Adsorption and Photodegradation of Methylene Blue. *Int. J. Biol. Macromol.* **2021**, *193* (PA), 721−733.
(20) Kaith, B. S.; Sharma, R.; Kalia, S. Guar Gum Based Biodegradable, Antibacterial and Electrically Conductive Hydrogels. *Int. J. Biol. Macromol.* **2015**, *75*, 266−275.
(21) Duan, J.; Gao, Y.; Huang, Y.; Li, L.; Jiang, J. Preparation and Characterization of a High Strength Self-Repairing Galactomannan Hydrogel. *BioResources* **2019**, *14* (4), 9853−9866.
(22) Sharma, R.; Kalia, S.; Kaith, B. S.; Srivastava, M. K. Synthesis of Guar Gum-Acrylic Acid Graft Copolymers Based Biodegradable Adsorbents for Cationic Dye Removal. *Int. J. Plast. Technol.* **2016**, *20* (2), 294−314.
(23) Pei, Y.; Chu, S.; Chen, Y.; Li, Z.; Zhao, J.; Liu, S.; Wu, X.; Liu, J.; Zheng, X.; Tang, K. Tannin-Immobilized Cellulose Hydrogel Fabricated by a Homogeneous Reaction as a Potential Adsorbent for Removing Cationic Organic Dye from Aqueous Solution. *Int. J. Biol. Macromol.* **2017**, *103*, 254−260.
(24) Vilela, C.; Moreirinha, C.; Almeida, A.; Silvestre, A. J. D.; Freire, C. S. R. Zwitterionic Nanocellulose-Based Membranes for Organic Dye Removal. *Materials* **2019**, *12* (9), 1404.
(25) Zafar, S.; Hanif, M.; Azeem, M.; Mahmood, K.; Gondal, S. A. Role of Crosslinkers for Synthesizing Biocompatible, Biodegradable and Mechanically Strong Hydrogels with Desired Release Profile. *Polym. Bull.* **2022**, *79* (11), 9199−9219.
(26) Tanpichai, S.; Phoothong, F.; Boonmahitthisud, A. Super-absorbent Cellulose-Based Hydrogels Cross-Liked with Borax. *Sci. Rep.* **2022**, *12* (1), 8920−9012.
(27) Sringam, J.; Trongsatitkul, T.; Suppakarn, N. Effects of Borax and Montmorillonite Contents on Mechanical Properties of Cassava Btarch-Based Composite Hydrogels. *AIP Conf. Proc.* **2020**, *2279* (October), 070005.
(28) Subrahmanyam, P. J. Design and Development of Guar Gum and Borax Crosslinked Guar Gum Matrix Tablets of Theophylline for Colon Specific Drug. *J. Chem. Pharmaceut. Res.* **2012**, *4* (2), 1052−1060.
(29) Hosseinpour, Z. H. Carboxyalkylated Cullulose Nanocrystals for Novel Applications. Doctor of Philosophy in Biotechnology, Lakehead University, 2021.
(30) Thakur, S.; Sharma, B.; Verma, A.; Chaudhary, J.; Tamulevicius, S.; Thakur, V. K. Recent Approaches in Guar Gum Hydrogel Synthesis for Water Purification. *Int. J. Polym. Anal. Charact.* **2018**, *23* (7), 621−632.
(31) Mahjoub, H. F.; Zammali, M.; Abbes, C.; Othman, T. Microrheological Study of PVA/Borax Physical Gels: Effect of Chain Length and Elastic Reinforcement by Sodium Hydroxide Addition. *J. Mol. Liq.* **2019**, *291*, 111272.
(32) Tanpichai, S.; Oksman, K. Cross-Linked Nanocomposite Hydrogels Based on Cellulose Nanocrystals and PVA: Mechanical Properties and Creep Recovery. *Composites, Part A* **2016**, *88*, 226−233.
(33) Geng, S.; Haque, M. M. U.; Oksman, K. Crosslinked Poly(Vinyl Acetate) (PVAc) Reinforced with Cellulose Nanocrystals (CNC): Structure and Mechanical Properties. *Compos. Sci. Technol.* **2016**, *126*, 35−42.
(34) Abd El-Mohdy, H. L.; Ghanem, S. Biodegradability, Antimicrobial Activity and Properties of PVA/PVP Hydrogels Prepared by γ-Irradiation. *J. Polym. Res.* **2009**, *16* (1), 1−10.
(35) Allouss, D.; Essamlali, Y.; Amadine, O.; Chakir, A.; Zahouily, M. Response Surface Methodology for Optimization of Methylene Blue Adsorption onto Carboxymethyl Cellulose-Based Hydrogel Beads: Adsorption Kinetics, Isotherm, Thermodynamics and Reusability Studies. *RSC Adv.* **2019**, *9* (65), 37858−37869.
(36) Andreas, A.; Winata, Z. G.; Santoso, S. P.; Angkawijaya, A. E.; Yuliana, M.; Soetaredjo, F. E.; Ismadji, S.; Hsu, H. Y.; Go, A. W.; Ju, Y. H. Biocomposite Hydrogel Beads from Glutaraldehyde-Crosslinked Phytochemicals in Alginate for Effective Removal of Methylene Blue. *J. Mol. Liq.* **2021**, *329*, 115579.
(37) Salazar-Rabago, J. J.; Leyva-Ramos, R.; Rivera-Utrilla, J.; Ocampo-Perez, R.; Cerino-Cordova, F. J. Biosorption Mechanism of Methylene Blue from Aqueous Solution onto White Pine (Pinus Durangensis) Sawdust: Effect of Operating Conditions. *Sustainable Environ. Res.* **2017**, *27* (1), 32−40.
(38) Chham, A.; Khouya, E.; Oumam, M.; Abourriche, A.; Gmouh, S.; Mansouri, S.; Elhammoudi, N.; Hanafi, N.; Hannache, H. The Use of Insoluble Matter of Moroccan Oil Shale for Removal of Dyes from Aqueous Solution. *Chem. Int.* **2019**, *4* (January), 67−76.
(39) Greluk, M.; Hubicki, Z. Comparison of the Gel Anion Exchangers for Removal of Acid Orange 7 from Aqueous Solution. *Chem. Eng. J.* **2011**, *170* (1), 184−193.
(40) Wang, J.; Meng, X.; Yuan, Z.; Tian, Y.; Bai, Y.; Jin, Z. Acrylated Composite Hydrogel Preparation and Adsorption Kinetics of Methylene Blue. *Molecules* **2017**, *22* (11), 1824−1912.
(41) Kumar, P. S.; Ramalingam, S.; Kirupha, S. D.; Murugesan, A.; Vidhyadevi, T.; Sivanesan, S. Adsorption Behavior of Nickel(II) onto Cashew Nut Shell: Equilibrium, Thermodynamics, Kinetics, Mechanism and Process Design. *Chem. Eng. J.* **2011**, *167* (1), 122−131.
(42) Abdul Khalil, H. P. S.; Saurabh, C. K.; Tye, Y. Y.; Lai, T. K.; Easa, A. M.; Rosamah, E.; Fazita, M. R. N.; Syakir, M. I.; Adnan, A. S.; Fizree, H. M.; Aprilia, N. A. S.; Banerjee, A. Seaweed Based Sustainable Films and Composites for Food and Pharmaceutical Applications: A Review. *Renew. Sustain. Energy Rev.* **2017**, *77* (September 2016), 353−362.
(43) Kaith, B. S.; Sharma, R.; Kalia, S.; Bhatti, M. S. Response Surface Methodology and Optimized Synthesis of Guar Gum-Based Hydrogels with Enhanced Swelling Capacity. *RSC Adv.* **2014**, *4* (76), 40339−40344.
(44) Singha, N. R.; Dutta, A.; Mahapatra, M.; Karmakar, M.; Mondal, H.; Chattopadhyay, P. K.; Maiti, D. K. Guar Gum-Grafted Terpolymer Hydrogels for Ligand-Selective Individual and Synergistic Adsorption: Effect of Comonomer Composition. *ACS Omega* **2018**, *3* (1), 472−494.
(45) Anjum, F.; Gul, S.; Khan, M. I.; Khan, M. A. Efficient Synthesis of Palladium Nanoparticles Using Guar Gum as Stabilizer and Their Applications as Catalyst in Reduction Reactions and Degradation of Azo Dyes. *Green Process. Synth.* **2019**, *9* (1), 63−76.
(46) Dassanayake, R. S.; Rajakaruna, E.; Abidi, N. Borax-Cross-Linked Guar Gum-Manganese Dioxide Composites for Oxidative Decolorization of Methylene Blue. *J. Nanomater.* **2019**, *2019*, 1−11.
(47) Lei, C.; Clark, P. E. Crosslinking of Guar and Guar Derivatives. *SPE J.* **2007**, *12* (03), 316−321.
(48) Li, Z.; Xu, W.; Wang, X.; Jiang, W.; Ma, X.; Wang, F.; Zhang, C.; Ren, C. Fabrication of PVA/PAAm IPN Hydrogel with High Adhesion and Enhanced Mechanical Properties for Body Sensors and

https://doi.org/10.1021/acsomega.3c06924
ACS Omega 2024, 9, 8904−8922

Antibacterial Activity. *Eur. Polym. J.* **2021**, *146* (December 2020), 110253.
(49) Arno, M. C.; Inam, M.; Weems, A. C.; Li, Z.; Binch, A. L. A.; Platt, C. I.; Richardson, S. M.; Hoyland, J. A.; Dove, A. P.; O'Reilly, R. K. Exploiting the Role of Nanoparticle Shape in Enhancing Hydrogel Adhesive and Mechanical Properties. *Nat. Commun.* **2020**, *11* (1), 1420.
(50) Sharma, R.; Kaith, B. S.; Kalia, S.; Pathania, D.; Kumar, A.; Sharma, N.; Street, R. M.; Schauer, C. Biodegradable and Conducting Hydrogels Based on Guar Gum Polysaccharide for Antibacterial and Dye Removal Applications. *J. Environ. Manage.* **2015**, *162*, 37−45.
(51) Li, S.; Zhang, H.; Feng, J.; Xu, R.; Liu, X. Facile Preparation of Poly(Acrylic Acid-Acrylamide) Hydrogels by Frontal Polymerization and Their Use in Removal of Cationic Dyes from Aqueous Solution. *Desalination* **2011**, *280* (1−3), 95−102.

https://doi.org/10.1021/acsomega.3c06924
ACS Omega 2024, 9, 8904−8922